

Original Paper

Petroleum geochemistry and origin of shallow-buried saline lacustrine oils in the slope zone of the Mahu sag, Junggar Basin, NW China

Dong-Yong Wang^{a, b}, Mei-Jun Li^{a, b, *}, Yang Zhou^{c, **}, Lu Yang^d, Yuan-Feng Yang^e, Er-Ting Li^f, Jun Jin^f, Xian-Li Zou^g, Bo-Dong Xu^g

^a State Key Laboratory of Petroleum Resources and Prospecting, China University of Petroleum (Beijing), Beijing, 102249, China

^b College of Geosciences, China University of Petroleum (Beijing), Beijing, 102249, China

^c College of Chemistry and Environmental Engineering, Sichuan University of Science and Engineering, Zigong, 643000, Sichuan, China

^d College of Resources and Environment, Chengdu University of Information Technology, Chengdu, 610225, Sichuan, China

^e Baikouquan Oil Production Plant, Xinjiang Oilfield Company CNPC, Karamay, 834000, Xinjiang, China

^f Research Institute of Experiment and Detection of Xinjiang Oilfield Company CNPC, Karamay, 834000, Xinjiang, China

^g Faculty of Petroleum, China University of Petroleum (Beijing) at Karamay, Karamay, 834000, Xinjiang, China

ARTICLE INFO

Article history:

Received 17 February 2023

Received in revised form

11 April 2023

Accepted 20 August 2023

Available online xxx

Edited by Jie Hao and Teng Zhu

Keywords:

Molecular marker

Saline lacustrine oil

Petroleum origin

Lower Permian Fengcheng Formation

Shallow-buried reservoir

Mahu Sag

ABSTRACT

Recently, significant oil discoveries have been made in the shallower pay zones of the Jurassic Badaowan Formation (J_{1b}) in the Mahu Sag, Junggar Basin, Northwest China. However, little work has been done on the geochemical characteristics and origins of the oil in the J_{1b} reservoir. This study analyzes 44 oil and 14 source rock samples from the area in order to reveal their organic geochemical characteristics and the origins of the oils. The J_{1b} oils are characterized by a low Pr/Ph ratio and high β -carotene and gammacerane indices, which indicate that they were mainly generated from source rocks deposited in a hypersaline environment. The oils are also extremely enhanced in C_{29} regular steranes, possibly derived from halophilic algae. Oil-source correlation shows that the oils were derived from the Lower Permian Fengcheng Formation (P_{1f}) source rocks, which were deposited in a strongly stratified and highly saline water column with a predominance of algal/bacterial input in the organic matter. The source rocks of the Middle Permian lower-Wuerhe Formation (P_{2w}), which were deposited in fresh to slightly saline water conditions with a greater input of terrigenous organic matter, make only a minor contribution to the J_{1b} oils. The reconstruction of the oil accumulation process shows that the J_{1b} oil reservoir may have been twice charged during Late Jurassic–Early Cretaceous and the Paleogene–Neogene, respectively. A large amount volume of hydrocarbons generated in the P_{1f} source rock and leaked from T_{1b} oil reservoirs migrated along faults connecting source beds and shallow-buried secondary faults into Jurassic traps, resulting in large-scale accumulations in J_{1b} . These results are crucial for understanding the petroleum system of the Mahu Sag and will provide valuable guidance for petroleum exploration in the shallower formations in the slope area of the sag.

© 2023 The Authors. Publishing services by Elsevier B.V. on behalf of KeAi Communications Co. Ltd. This is an open access article under the CC BY-NC-ND license (<http://creativecommons.org/licenses/by-nc-nd/4.0/>).

1. Introduction

Comparatively low drilling and operating costs and high efficiency in recovery endow petroleum resources in shallow strata with a special attraction for prospectors (Taylor, 1967; Wang et al.,

2012; Peng et al., 2013; Mi et al., 2018; Liang et al., 2020; Hackley et al., 2021). The Junggar Basin is regarded as one of the most prolific oil-producing basins in Northwest China (Fig. 1a). The Mahu Sag is one of the most hydrocarbon-abundant sags in the basin, with the slope zones hosting major hydrocarbon accumulations (Fig. 1b). Hydrocarbons have been produced from the fault zone in the northwestern part of the Junggar Basin since the 1950s (Chen et al., 2020). In the early 2010s, a major breakthrough in Lower Triassic Baikouquan (T_{1b}) glutenite triggered a renaissance for the Triassic plays in the basin, which have estimated recoverable oil reserves of more than 1 billion tons (Tang et al., 2019). The western

* Corresponding author. State Key Laboratory of Petroleum Resources and Prospecting, China University of Petroleum (Beijing), Beijing, 102249, China.

** Corresponding author.

E-mail addresses: meijunli@cup.edu.cn (M.-J. Li), zhouy@caep.ac.cn (Y. Zhou).

<https://doi.org/10.1016/j.petsci.2023.08.024>

1995-8226/© 2023 The Authors. Publishing services by Elsevier B.V. on behalf of KeAi Communications Co. Ltd. This is an open access article under the CC BY-NC-ND license (<http://creativecommons.org/licenses/by-nc-nd/4.0/>).

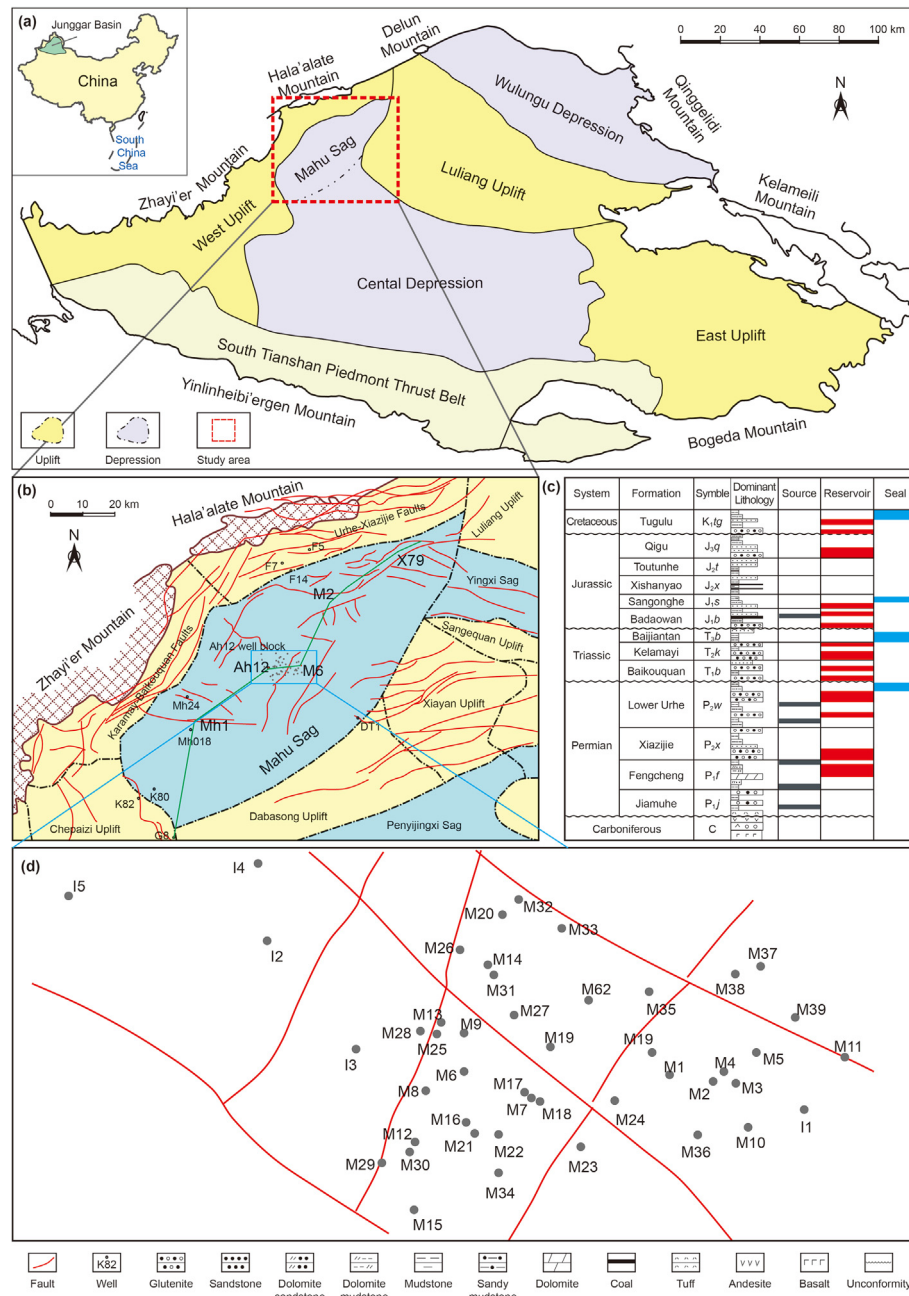


Fig. 1. (a) Structural units and location of the study area in the basin; (b) simplified tectonic framework of the Mahu Sag; (c) Comprehensive stratigraphic column of the Mahu Sag, including symbols, dominant lithologies and main petroleum system elements; and (d) location of sampled oil wells in the Ah 12 well block of the Mahu Sag.

slope zone of the Mahu Sag has accordingly become the leading oil-producing region in the Junggar Basin (Abulimit et al., 2016; D. Li et al., 2020). To further increase hydrocarbon production, the middle-shallow J_1b Formation in the sag has gradually become a favored petroleum exploration target. The shallow drilling depths (less than ~2000 m vertical depth) of the J_1b reservoir and cumulative production of over 10 million tons provide strong incentives for further development of the middle-shallow oil plays. This oil-source rock correlation study should therefore be viewed in the context of a broader investigation of the shallow-strata petroleum system in the basin (Qian et al., 2018). Previous studies have mainly focused on the spatial distribution and basic conditions of the J_1b oil accumulations. The main factors controlling oil accumulation and regional distribution in the shallow strata are the favorable

reservoir conditions, strike-slip faults, and high-quality source rocks (Chen et al., 2018; Song et al., 2019).

The origin of T_1b oils remains a controversial issue. Previous studies suggest that the T_1b oil might mostly originate from the P_1f source rock (e.g. Yu et al., 2018; Xiao et al., 2021). While the molecular markers, carbon isotopic compositions as well as trace element data show that the Triassic reservoir oils were possibly derived from a mixture of P_1f and Permian lower-Wuerhe Formation (P_2w) source rocks (Z. Chen et al., 2016; Liu et al., 2016; Chen et al., 2017). Some other studies show that the Early Permian Jiamuhe Formation (P_1j) contributed to the T_1b oil (e.g. Cao et al., 2005). In recent literature, Zhang et al. (2022) and Cai et al. (2023) reported that the discovered oils in the Mahu Sag can be divided into three groups based on the $\delta^{13}C$ values of individual n -

alkanes, i.e. group I, group II and group III, sourced from P_{1f}, P_{2w} and the mixture of both source beds, respectively. Previous studies have found that the J_{1b} and T_{1b} oils have similar source affinities (Hu et al., 2020), but this has not yet been verified by systematic geochemical analysis.

Based on petroleum geochemical data from 44 crude oil samples and 14 source rock samples, this paper investigates the geochemical characteristics and origin of the J_{1b} oils in the shallow-buried reservoirs in the Mahu Sag of the Junggar Basin. The results of this study will significantly improve understanding of the Jurassic petroleum system, constrain exploration risk, and improve exploration success in the shallow strata of the slope of the Mahu Sag.

2. Geological settings

The Junggar basin is one of the major petroliferous basins of Northwest China (Fig. 1a). It covers an area of about 38×10^4 km². It has been divided into several primary tectonic units and secondary structural units. The Mahu Sag, covering an area of ca. 5000 km², is located in the northwest of the Junggar Basin, bounded by the Karamay-Baikouquan Fault in the west, the Wuerhe-Xiazijie Fault in the north, and the western section of the Luliang Uplift in the east (Fig. 1b). It has experienced three tectonic evolution cycles (He et al., 2018). The initial phase, an oceanic basin cycle in the Devonian-early Carboniferous, resulted in the formation of a foreland basin. During a second cycle of extensional and contractional tectonics (Late Carboniferous to Triassic), marine-continental transitional sequences and deposition of terrigenous siliciclastic, evaporites, and carbonates occurred in the area. Finally, during the Jurassic to Quaternary, a lacustrine regression occurred, coinciding with deposition of fluvial delta (He et al., 2018). The study area has an NW-SE axis trend, with predominantly NW-SE trending faults, as well as some NE-SW and E-W faults (Fig. 1b). Four main erosional periods have been identified in this area that have resulted in a number of key regional unconformities (Ma et al., 2015) (Fig. 1c).

The Carboniferous basement consists of felsic to mafic rocks, including granites, granodiorites, diorites, and gneisses as well as metasediments and metavolcanics (Li et al., 2015, 2016, 2020; Zhao et al., 2019; J. Li et al., 2020). The Mahu Sag is considered to be overfilled, with multiple sets of source rocks. Based on their geological, geochemical and paleoenvironmental characteristics, four main potential source rock beds have been recognized in the marine-continental, transitional, and continental sequences of the sag. These are: the Carboniferous (C), the Lower Permian Jiamuhe Formation (P_{1j}), the Lower Permian Fengcheng Formation (P_{1f}), and the Middle Permian lower-Wuerhe Formation (P_{2w}) (Fig. 1c), (He et al., 2010; Feng et al., 2020). The tectonic movement of Late Permian resulted in the absence of upper-Wuerhe Formation (P_{3w}). The marine-continental transitional sequence is Carboniferous, deposited in a reducing environment. The continental sequence is composed of the P_{1j}, P_{1f}, and P_{2w} Formations, which—particularly P_{1f}—were deposited in a hypersaline lacustrine environment (Fig. 1b) and (Cao et al., 2015, 2020; Gao et al., 2018; Wang et al., 2021). P_{2w} and P_{1f} are considered to be the main potential source rocks for the oil discovered so far, with C and P_{1j} being regarded as potential gas source rocks. The main reservoir development pay zones within the Triassic are associated with the Triassic Baikouquan Formation (T_{1b}), which is composed of fan delta front glutenite (Jia et al., 2017; Wu et al., 2020; Liu et al., 2022) (Fig. 1b), with secondary reservoirs in delta deposits of the Triassic Delamanid Formation (T_{2k}) and the Jurassic Badaowan Formation (J_{1b}). Major discoveries and obvious hydrocarbon shows have been recorded in T_{1b} (Tang et al., 2019). The regional cap rocks for the Mahu sag

consist of P_{2w}, the Late Triassic Baijiania Formation (T_{3b}), the Jurassic Mishandle Formation (J_{1x}), and the Cretaceous Lugulu Group (K_{1tg}) (Fig. 1c).

3. Samples and experiments

3.1. Samples

Fourteen source rock core samples were selected from nine wells for geochemical analysis, including total organic carbon (TOC) content measurement, Rock-Eval pyrolysis, and gas chromatography–mass spectrometry (GC–MS). Similar geochemical analyses were conducted on 44 J_{1b} oil samples from 44 wells in the Ah12 well block. The locations of sampled oil wells are shown in Fig. 1d. Detailed information on geological settings and stratigraphy is shown in Fig. 1c.

3.2. Rock-Eval pyrolysis and TOC measurements

The source rock samples were ground into powder with particle diameters of less than 0.2 mm. Approximately 100 mg of each powdered sample was weighed and treated with diluted HCl to remove inorganic carbon. Other contaminants were removed by washing with deionized water for two days. Finally, all samples were dried in an oven at 80 °C for 24 h. The samples were then heated to 900 °C using a LECO CS-230 analyzer so that organic carbon was fully combusted and converted into carbon dioxide. Pyrolysis of the 100 mg source rock samples was carried out using an OGE-II, and the pyrolysis parameters (Table 1) were obtained.

3.3. GC–MS

Soluble organic matter was obtained by extracting source rock samples for 3 days using Soxhlet extraction. The soluble organic matter and oil samples were dissolved in 50 mL of petroleum ether, and then filtered through a funnel stuffed with a little clean cotton to remove insoluble compounds (asphaltenes). The saturated hydrocarbon fractions, aromatic hydrocarbon fractions, and resin fractions were obtained from the residual solutions using a silica gel/alumina standard chromatography column washed by sequential addition of petroleum ether, a mixed reagent of dichloromethane and petroleum ether (2:1, v:v), and a mixed reagent of dichloromethane and methanol (93:7, v:v).

The results presented in this study are based on geochemical parameters calculated from the saturated and aromatic fractions of crude oils obtained by GC–MS. GC–MS analyses of the saturated fractions were carried out on a 5975 A instrument, equipped with an HP-5MS chromatographic column (60 m length, 0.25 mm inner diameter, and 0.25 µm film thickness). Helium (purity > 99.999%) was used as the carrier gas. The oven temperature was initially set at 50 °C, with a 1 min hold. It was then raised to 120 °C at 20 °C/min during the first stage, and then to 310 °C at 3 °C/min during the second stage, where it was held for 20 min. Electron impact ionization (70 eV) was employed.

GC–MS analyses of the aromatic fractions were carried out using a 5977 A instrument, equipped with an HP-5MS chromatographic column (60 m length, 0.25 mm inner diameter, and 0.25 µm film thickness). Helium (purity > 99.999%) was used as the carrier gas. The initial oven temperature was set at 80 °C, held for 1 min and then raised to 310 °C at 3 °C/min, where it was held for 20 min. The mass spectrometer was operated in full scan, electron impact mode with electron energy of 70 eV.

Table 1
Bulk geochemical parameters of source rock samples in the study area.

Well	Sample ID	Formation	Depth, m	TOC, %	S_1 , mg/g	S_2 , mg/g	PG, mg/g	HI, mg/g	T_{max} , °C	R_o , %
F5	F1	P _{1f}	3470.90	0.63	0.54	7.05	7.59	817.05	441	0.89
	F2		3473.60	0.73	0.86	2.99	3.85	794.32	447	1.01
	F3		3476.10	0.40	0.34	1.11	1.45	662.12	454	1.15
F7	F4		3156.16	1.74	0.90	8.51	9.41	490.49	436	nd
	F5		3157.50	3.60	0.51	33.47	33.98	805.92	442	1.05
	F6		3182.90	1.34	0.85	6.66	7.51	498.50	433	nd
	F7		3220.55	0.44	1.40	7.89	9.29	585.71	438	0.96
	F8		3222.30	3.43	2.32	39.90	42.24	688.46	440	1.11
FN14	F9	P _{2w}	4065.19	2.40	1.03	13.93	14.96	635.25	440	nd
DT1	F10		5693.89	0.66	0.40	0.29	0.69	104.55	457	nd
K82	F11		4084.30	0.71	1.79	1.86	3.65	261.97	445	nd
MH6	M1		3772.00	1.05	0.28	0.71	0.99	477.90	445	1.14
	M2		3773.00	0.60	0.19	0.79	0.98	267.62	455	1.20
K80	M3		4084.00	0.55	0.16	0.88	0.24	160.00	457	nd

Notes: TOC: Total organic matter content; S_1 : volatile hydrocarbon (HC) content; S_2 : remaining (HC) generative potential; PG: genetic potential = ($S_1 + S_2$); HI: Hydrogen index = $S_2 \times 100/\text{TOC}$; T_{max} : temperature at maximum generation; R_o : vitrinite reflectance; nd: no data.

4. Results and discussions

4.1. Geochemical characteristics of potential source rocks

The total organic carbon (TOC) content of the P_{1f} source rocks ranges from 0.40 wt.% to 3.60 wt.%, with a mean of 1.46 wt.%, indicating high organic matter abundance in all samples (Fig. 2a). The hydrocarbon generating potential ($S_1 + S_2$) of the P_{1f} source rocks ranges in value from 0.69 to 42.24 mg/g, with a mean of 12.24 mg/g (Fig. 2a). The samples from the P_{1f} Formation can therefore be classified as moderate to excellent source rocks (Peters, 1986) (Fig. 2a). The TOC values of the P_{2w} source rocks are lower, with an average of 0.73 wt.%, indicating lower organic matter abundance (Table 1). The samples from the P_{2w} Formation are therefore poor source rocks, as shown in Fig. 2a. The HI values of the P_{1f} source rocks range from 104.55 to 817.05 mg HC/g TOC, suggesting Type I kerogen progenitors for this interval (Tissot and Welte, 1984; Espitalié et al., 1985a) (Fig. 2b). However, the samples from the P_{2w} Formation fall within the zone of type II₁ kerogen on the HI- T_{max} graph (Fig. 2b).

The temperature at the S_2 peak of programmed pyrolysis (T_{max}) values of P_{1f} ranged from 436 °C to 457 °C (Fig. 2b), indicating that the maturity range of the organic matter was from mature

($R_o = 0.5$ –1.2%) to high mature ($R_o = 1.2$ %–2.0%) (Peters and Cassa, 1994; Espitalié et al., 1985b). The T_{max} of the P_{2w} samples showed an average of 452 °C, suggesting that the organic matter in the formation has entered the oil generation window (Fig. 2b).

Overall, the results indicate that the organic matter in the P_{1f} Formation has generally good to excellent hydrocarbon generation potential, corresponding to Type I kerogen (Fig. 2). However, the overlying P_{2w} source rocks are comparatively poor, with the results being consistent with Type II₁ kerogen (Fig. 2). The maturity of the Permian source rocks increases from mature to high-mature in the study area and both sets are potential source rocks for the sampled oils.

4.2. Maturity assessment

The OEP (Odd-Even Predominance) and CPI (Carbon Preference Index) values of all oil samples are around one with an average of 1.05 and 1.06, respectively, indicating these oils were generated by source rocks in mature stage. All oils have C₃₁αβ hopane 22 S/(S + R) ratios approaching equilibrium points with a mean of 0.60, which suggests mature oils (Zumberge, 1987). All oil samples with a mean of C₂₉ααα sterane 20 S/(S + R) of 0.50 and a mean of C₂₉ sterane αββ/(ααα+αββ) of 0.61 reaching equilibrium suggest a high

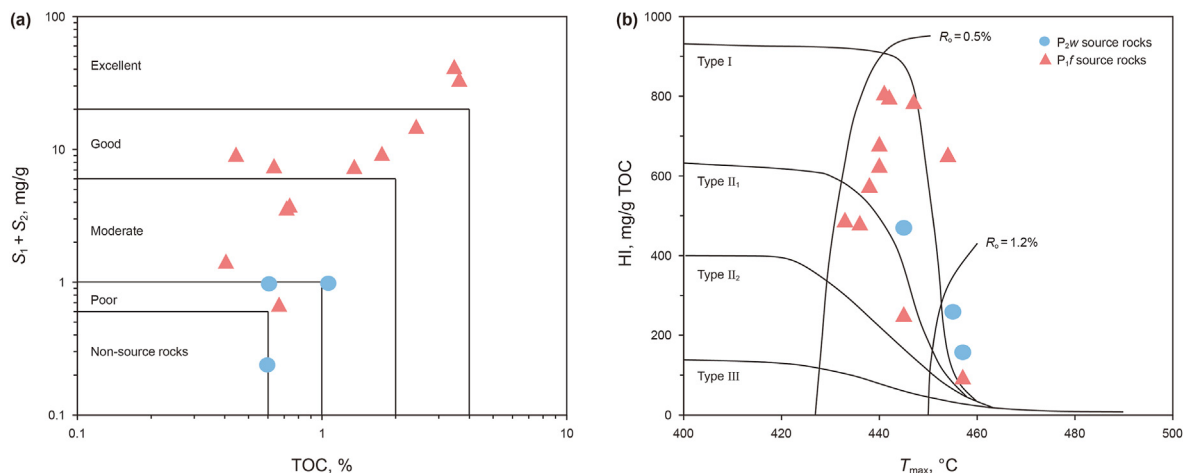


Fig. 2. Organic matter characterization of the P_{1f} and P_{2w} source rock samples was carried out using: (a) the relationship between TOC and $S_1 + S_2$; and (b) the relationship between the HI and temperature of peak pyrolysis generation (T_{max}) to reveal the kerogen types.

Table 2Parameters of *n*-alkanes and acyclic isoprenoids from source rock extracts and oils in the study area.

Sample ID	Sample Type	Pr/ <i>n</i> -C ₁₇	Ph/ <i>n</i> -C ₁₈	Pr/Ph	C _{max}	β-Carotane/C _{max}	CPI	OEP	R _c	R _{ca}
F1	Core	1.63	5.58	0.44	<i>n</i> -C ₁₇	2.30	1.05	1.04	1.45	0.86
F2	Core	1.40	5.15	0.44	<i>n</i> -C ₁₇	1.52	1.02	1.03	1.45	0.91
F3	Core	2.17	5.58	0.52	<i>n</i> -C ₁₇	9.27	1.05	1.06	1.29	1.10
F4	Core	1.17	1.81	0.64	<i>n</i> -C ₁₇	4.83	1.03	1.05	1.42	1.39
F5	Core	0.65	0.98	0.80	<i>n</i> -C ₂₀	0.59	1.05	1.05	1.39	1.18
F6	Core	0.97	1.88	0.57	<i>n</i> -C ₁₇	0.48	1.06	1.06	1.49	1.17
F7	Core	0.55	1.40	0.63	<i>n</i> -C ₁₇	0.85	1.04	1.03	1.57	0.97
F8	Core	1.44	2.82	0.36	<i>n</i> -C ₁₇	4.15	1.04	1.05	1.49	1.02
F9	Core	0.93	1.27	0.83	<i>n</i> -C ₁₇	2.14	1.04	1.06	1.48	1.51
F10	Core	0.66	0.80	0.81	<i>n</i> -C ₁₇	1.39	1.03	1.04	2.64	1.18
F11	Core	0.62	0.98	0.82	<i>n</i> -C ₁₇	0.01	1.06	1.03	1.05	0.84
W1	Core	0.34	0.69	1.39	<i>n</i> -C ₁₇ , <i>n</i> -C ₂₅	0.06	1.05	1.06	0.95	0.91
W2	Core	0.51	0.65	1.04	<i>n</i> -C ₁₆ , <i>n</i> -C ₂₇	0.03	1.03	1.02	1.04	0.71
W3	Core	0.48	0.56	0.84	<i>n</i> -C ₁₆ , <i>n</i> -C ₂₅	0.03	1.06	1.05	1.00	0.96
M1	Oil	1.46	1.05	0.76	<i>n</i> -C ₁₇	0.72	1.05	1.05	0.69	0.56
M2	Oil	1.46	1.05	0.76	<i>n</i> -C ₁₇	0.81	1.06	1.06	0.73	0.60
M3	Oil	1.51	1.05	0.74	<i>n</i> -C ₁₇	0.74	1.05	1.06	0.70	0.58
M4	Oil	1.39	1.05	0.79	<i>n</i> -C ₁₇	0.74	1.04	1.04	0.73	0.63
M5	Oil	1.50	1.05	0.74	<i>n</i> -C ₁₇	0.77	1.06	1.05	0.70	0.57
M6	Oil	1.52	1.09	0.76	<i>n</i> -C ₁₇	0.65	1.07	1.04	0.76	0.65
M7	Oil	1.46	1.07	0.75	<i>n</i> -C ₁₇	0.75	1.06	1.04	0.72	0.56
M8	Oil	1.45	1.04	0.75	<i>n</i> -C ₁₇	0.90	1.07	1.05	0.71	0.54
M9	Oil	1.82	1.36	0.77	<i>n</i> -C ₁₇	0.64	1.06	1.03	0.89	0.78
M10	Oil	1.47	1.06	0.76	<i>n</i> -C ₂₀	0.85	1.07	1.05	0.72	0.58
M11	Oil	1.47	1.06	0.76	<i>n</i> -C ₁₇	0.82	1.08	1.05	0.73	0.56
M12	Oil	1.54	1.12	0.77	<i>n</i> -C ₁₇	0.55	1.06	1.06	0.71	0.56
M13	Oil	1.53	1.09	0.75	<i>n</i> -C ₁₇	0.74	1.06	1.04	0.71	0.59
M14	Oil	1.49	1.08	0.77	<i>n</i> -C ₁₇	0.69	1.06	1.05	0.72	0.55
M15	Oil	1.75	1.34	0.79	<i>n</i> -C ₁₇	0.54	1.06	1.04	0.80	0.68
M16	Oil	1.53	1.13	0.77	<i>n</i> -C ₁₇	0.58	1.06	1.04	0.79	0.53
M17	Oil	1.46	1.06	0.76	<i>n</i> -C ₁₇	0.80	1.04	1.06	0.75	0.54
M18	Oil	1.50	1.08	0.72	<i>n</i> -C ₂₀	0.89	1.06	1.05	0.71	0.53
M19	Oil	1.51	1.10	0.75	<i>n</i> -C ₂₀	0.81	1.05	1.06	0.77	0.56
M20	Oil	1.86	1.35	0.75	<i>n</i> -C ₁₇	0.61	1.04	1.05	0.86	0.71
M21	Oil	1.53	1.18	0.80	<i>n</i> -C ₁₇	0.59	1.06	1.05	0.64	0.53
M22	Oil	1.54	1.15	0.78	<i>n</i> -C ₁₇	0.65	1.04	1.06	0.64	0.54
M23	Oil	1.60	1.26	0.79	<i>n</i> -C ₂₀	0.60	1.07	1.05	0.62	0.52
M24	Oil	1.49	1.07	0.77	<i>n</i> -C ₁₇	0.69	1.06	1.06	0.63	0.56
M25	Oil	1.47	0.97	0.66	<i>n</i> -C ₂₀	1.11	1.07	1.08	0.78	0.54
M26	Oil	1.51	1.04	0.71	<i>n</i> -C ₂₀	0.88	1.06	1.07	0.76	0.57
M27	Oil	1.50	1.03	0.71	<i>n</i> -C ₂₀	0.76	1.07	1.07	0.75	0.57
M28	Oil	1.54	1.13	0.77	<i>n</i> -C ₁₇	0.66	1.06	1.06	0.76	0.55
M29	Oil	1.48	1.09	0.75	<i>n</i> -C ₁₇	0.76	1.09	1.06	0.69	0.53
M30	Oil	1.53	1.15	0.76	<i>n</i> -C ₁₇	0.70	1.07	1.05	0.72	0.53
M31	Oil	1.53	1.04	0.70	<i>n</i> -C ₁₉	0.89	0.93	0.74	0.75	0.53
M32	Oil	1.55	1.05	0.70	<i>n</i> -C ₂₀	0.71	1.05	1.07	0.74	0.54
M33	Oil	1.49	1.05	0.80	<i>n</i> -C ₂₁	0.76	1.08	1.11	0.77	0.53
M34	Oil	1.49	1.08	0.73	<i>n</i> -C ₂₀	0.82	1.08	1.05	0.74	0.54
M35	Oil	1.53	1.06	0.73	<i>n</i> -C ₂₀	0.76	1.06	1.06	0.71	0.56
M36	Oil	1.50	1.09	0.75	<i>n</i> -C ₂₀	0.66	1.06	1.05	0.73	0.54
M37	Oil	1.49	1.04	0.74	<i>n</i> -C ₁₇	0.78	1.07	1.06	0.72	0.52
M38	Oil	1.52	1.10	0.74	<i>n</i> -C ₂₀	0.74	1.05	1.05	0.68	0.53
M39	Oil	1.51	1.11	0.76	<i>n</i> -C ₂₀	0.78	1.07	1.07	0.67	0.51
I1	Oil	1.48	1.06	0.80	<i>n</i> -C ₂₀	0.89	1.05	1.10	0.70	0.57
I2	Oil	1.60	1.27	0.82	<i>n</i> -C ₁₇	0.79	1.07	1.04	0.78	0.76
I3	Oil	1.55	1.11	0.75	<i>n</i> -C ₁₇	0.91	1.08	1.06	0.69	0.54
I4	Oil	1.82	1.37	0.81	<i>n</i> -C ₁₇	0.52	1.07	1.06	0.81	0.97
I5	Oil	1.91	1.48	0.80	<i>n</i> -C ₂₀	0.54	1.04	1.05	0.67	0.55

Notes: Pr/*n*-C₁₇: Pristane/*n*-C₁₇; Ph/*n*-C₁₈: Phytane/*n*-C₁₈; Pr/Ph: Pristane/Phytane; C_{max}: The carbon number of maximum peak; β-Carotane/C_{max}: β-Carotane/The carbon number of maximum peak; CPI: [(C₂₅ + C₂₇ + C₂₉ + C₃₁ + C₃₃)/1]/[(C₂₄ + C₂₆ + C₂₈ + C₃₀ + C₃₂) + 1]/[(C₂₆ + C₂₈ + C₃₀ + C₃₂ + C₃₄)]^m; OEP: [(C_i + 6C_{i+2} + C_{i+4})/(4C_{i+1} + 4C_{i+3})]^m, *m* = (-1)ⁱ⁺¹, *i* = C_{max}; R_c(%): 0.40 + 0.60 × MPI-1, MPI-1 = 1.5 × (2-MP + 3-MP)/(P + 1-MP + 9-MP), P = Phenanthrene, MP = Methylphenanthrene; R_{ca}(%): 0.49 + 0.09 × DNR, DNE = (2,6- + 2,7-)/1,5-dimethylnaphthalene.

thermal evolution. The R_c% equivalent calculated by methylphenanthrene index amount to 0.67%–0.89% with a mean of 0.73% (Table 2), suggesting oils are in mature stage (Radke et al., 1986). The R_{ca} (%) for all oils is between 0.51% and 0.97% [R_{ca} (%) = 0.49 + 0.09 × DNR (DNR = (2,6- + 2,7-)/1,5-dimethylnaphthalene)] (Li et al., 2013, 2014). All maturation indicators suggest that the oil samples are in mature stage bearing a limited value range of thermal maturation levels.

4.3. Oil-oil and oil-source rock correlations

4.3.1. Normal-alkanes and acyclic isoprenoids

Generally, predominance of lower carbon number components is associated with organic matter input from mainly aquatic organisms (Peters et al., 2005), while long chain *n*-alkanes are mainly derived from terrigenous higher plants (Brooks and Smith, 1969). In this study, total ion chromatograms (TIC) of all oil samples reveal

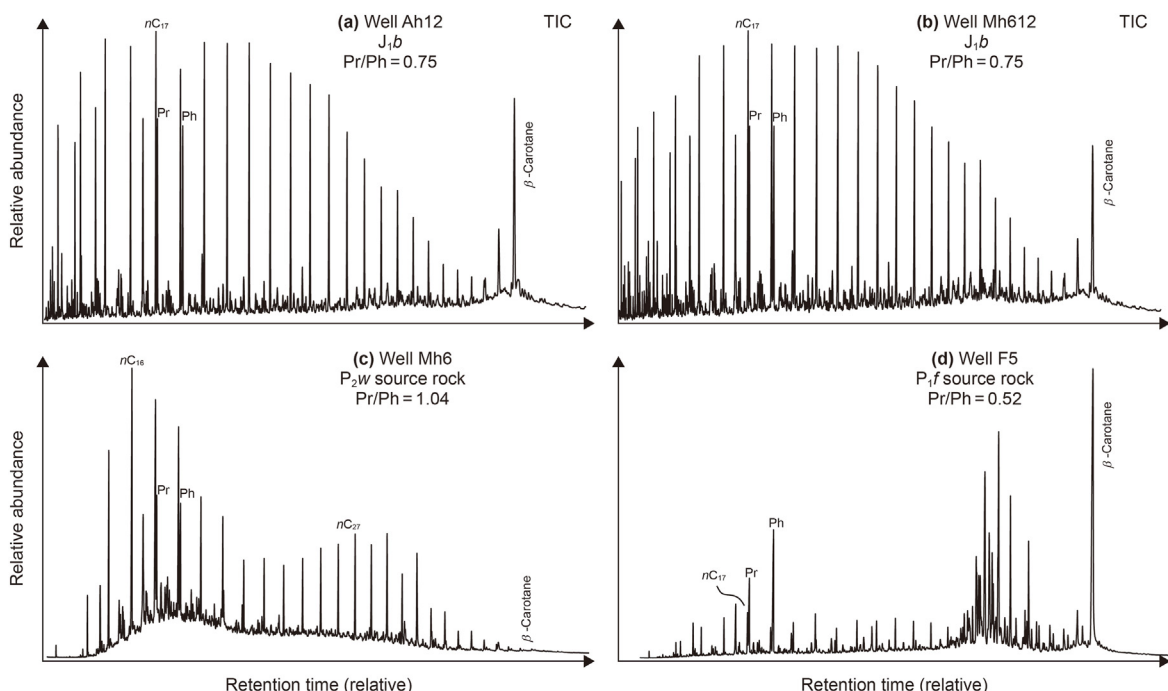


Fig. 3. Representative TIC of the saturated fractions showing the distribution of *n*-alkanes for (a) and (b) the *J*₁*b* oils, (c) solvent extracts of *P*₂*w* source rocks, and (d) solvent extracts of *P*₁*f* source rocks.

similar *n*-alkanes distribution patterns and acyclic isoprenoid contents. The carbon numbers typically range from *n*-C₁₂ to *n*-C₃₅. The distribution patterns of *n*-alkanes are unimodal, with the maximum peak generally close to *n*-C₁₇ (Table 2) and a gradual decrease in peak content with increasing carbon numbers (Fig. 3a and b). This *n*-alkanes distribution pattern is characteristic of source rocks with strong input from marine organic matter. However, TICs of solvent extracts from the *P*₂*w* source rocks are more variable than those of the *J*₁*b* oils and are distinctly bimodal, with maxima at *n*-C₁₇ and *n*-C₂₅ (Fig. 3c), indicating a mixture of terrestrial higher plants and aquatic organisms. Solvent extracts from the *P*₁*f* source rocks show unimodal patterns with maximum carbon peaks at *n*-C₁₇ (Fig. 3d; Table 2), indicating predominantly marine organic matter, as revealed by organic petrology (Xia et al., 2022; Hou et al., 2022). The *n*-alkanes distribution patterns suggest that the *J*₁*b* oils mainly originated from the *P*₁*f* source rocks (Fig. 3).

Low pristane/phytane (Pr/Ph) ratios (< 1.0) generally reflect marine organic matter input under anoxic conditions, while high Pr/Ph ratios (> 3.0) reflect an oxic depositional environment with more terrestrial organic matter (Brooks et al., 1969; Peters et al., 2005). All of the oil samples show uniform Pr/Ph ratios within the range 0.66–0.82 (Table 2), which is consistent with organic matter from aquatic organisms formed in a reducing environment. The Pr/Ph values (Peak area ratio) range from 0.84 to 1.39 (with an average of 1.09) for the *P*₂*w* solvent extracts, corresponding with aquatic organic material. The values for the *P*₂*w* solvent extracts are higher than those of the *J*₁*b* oils, suggesting that the *P*₂*w* source rocks were deposited in a relatively oxidizing water body. The Pr/Ph ratios of 0.36–0.83 in solvent extracts from the *P*₁*f* source rocks are also consistent with predominantly aquatic organisms in the organic matter. The results show that the Pr/Ph ratios of the *J*₁*b* oils are closer to those of the *P*₁*f* source rocks. The Pr/*n*-C₁₇ versus Ph/*n*-C₁₈ discriminant plot of all the oil samples (Fig. 4a) also indicates marine organic matter sources (Shanmugam, 1985). The Pr/*n*-C₁₇ and Ph/*n*-C₁₈ ratios for the *P*₂*w* source rocks suggest that they were deposited under reducing conditions with marine organic matter

input (Fig. 4a). The plotted values of Pr/*n*-C₁₇ and Ph/*n*-C₁₈ ratios for the *P*₁*f* source rocks also fall within the marine organic matter zone of the diagram (Fig. 4a). In the cross plot of Pr/*n*-C₁₇–Ph/*n*-C₁₈ (Fig. 4a), solvent extracts from the *P*₁*f* source rocks show certain variability but generally plot close to the *J*₁*b* oil samples. In the triangular diagram of acyclic alkane ratios (Pr/Ph, Pr/*n*-C₁₇, and Ph/*n*-C₁₈) (Fig. 4b), the data points of the *J*₁*b* oil samples and the *P*₁*f* source rock samples fall close together in one area, indicating a high degree of affinity between those oils and the *P*₁*f* source rocks. These indicators therefore suggest that the *P*₁*f* source rocks are likely to be the source for the *J*₁*b* oils.

4.3.2. β -carotane

High concentrations of β -carotane and γ -carotane were identified in TICs of the oils and source rocks in the study area (Fig. 3). These compounds can be positively identified in the *m/z* 125 mass chromatograms by comparing their relative retention times with the literature (Fig. 5) (Murphy et al., 1967). The relative abundance of β -carotane in the *P*₁*f* source rocks is significantly higher than that of *n*-alkanes (Fig. 3d; Fig. 5d), while the *P*₂*w* source rocks contain few of these compounds (Fig. 3c; Fig. 5c). Notably, the abundance of β -carotane in the *J*₁*b* oil samples is distinctly higher than in the *P*₂*w* source rocks (Fig. 3a and b; Fig. 5a and b). The β -carotane distribution patterns in the *P*₁*f* source rocks, on the other hand, closely match those of the oils (Fig. 3; Fig. 5).

β -Carotane is generally believed to originate from β -carotene. However, the exact biogenetic source of β -carotane remains a matter of debate, as β -carotane occurs in higher plants as well as in algae and bacteria. β -Carotane is commonly formed in highly saline, strongly reducing water bodies (Murphy et al., 1967; Moldowan et al., 1985; Hopmans et al., 2005; Peters et al., 2005; Ding et al., 2017, 2020), although there are minor exceptions to this general rule (Philp et al., 1992; Grba et al., 2014). In this study, the β -carotane index (β -carotane/*C*_{max}, *C*_{max}: maximum carbon peak in TIC) shows a negative correlation with the Pr/Ph ratios (Fig. 6), indicating that an anoxic depositional environment may be beneficial

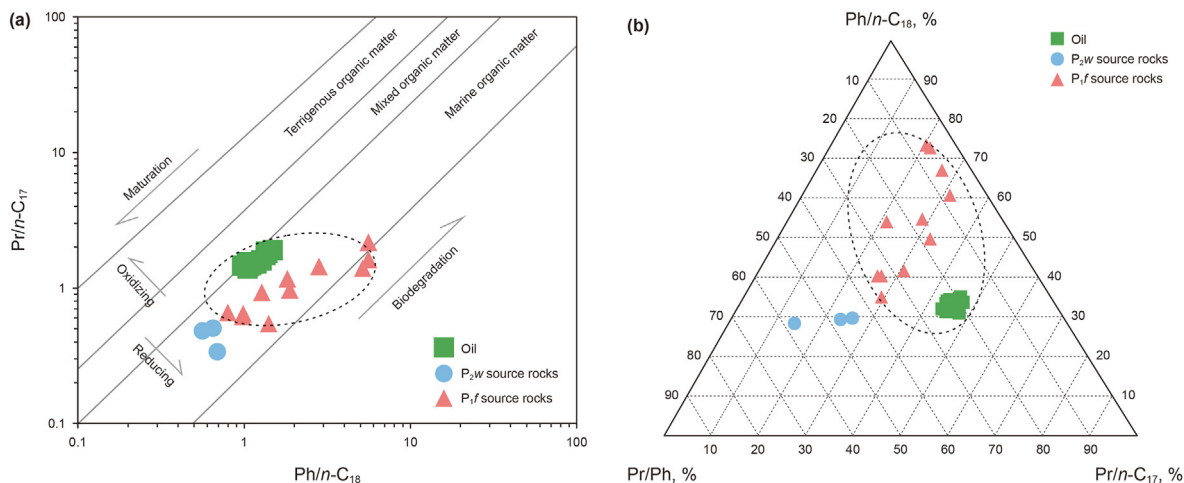


Fig. 4. (a) Cross plot of $\text{Ph}/n\text{-C}_{18}$ versus $\text{Pr}/n\text{-C}_{17}$ (b) triangular diagram of acyclic alkane ratios for the J_1b oil and Permian source rocks in the study area.

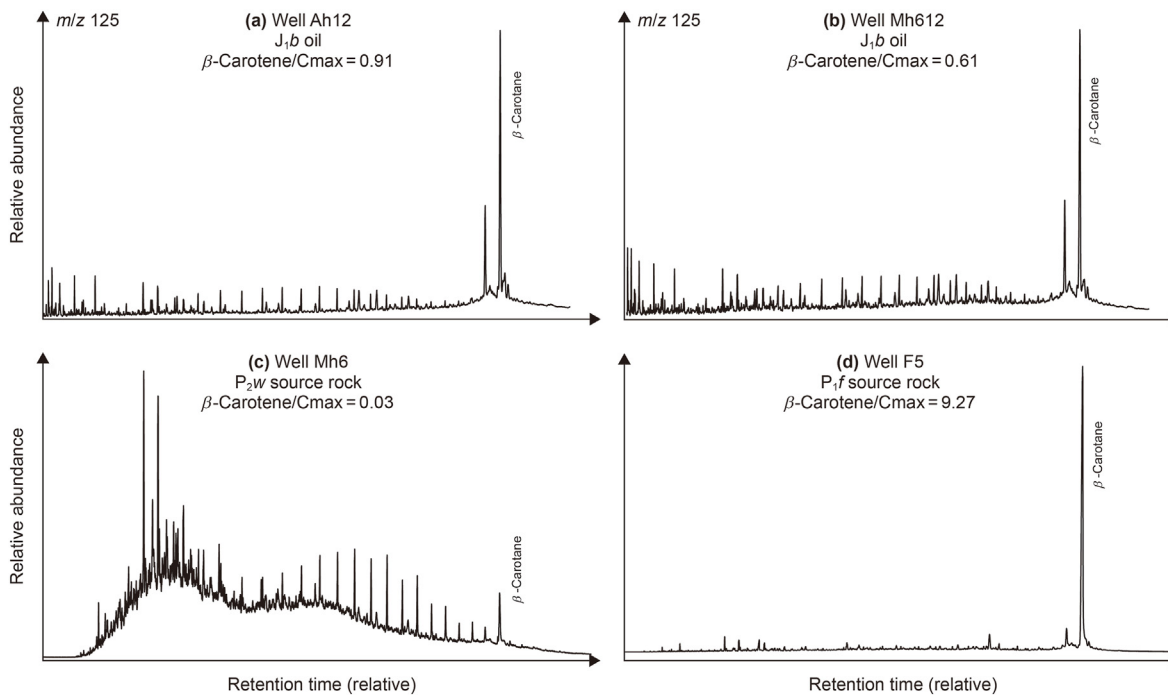


Fig. 5. Representative m/z 125 fragmentograms of the saturated fraction showing the distribution of β -carotene for (a) and (b) the J_1b oils, (c) solvent extracts of P_2w source rocks, and (d) solvent extracts of P_{1f} source rocks.

for the formation of β -carotene (Ding et al., 2020). In the cross plot of the β -carotene index and Pr/Ph ratios shown in Fig. 6, all the J_1b oil samples are plotted together, indicating a single oil family. They are also closely associated with the P_{1f} source rocks, but differ markedly from the solvent extracts from the P_2w source rocks (Fig. 6). The J_1b oils and the P_{1f} source rocks both have high β -carotene contents, again suggesting that the J_1b oils were generated from the P_{1f} source rocks.

4.3.3. Hopane series

Hopanes and their derivatives were also identified in m/z 191 mass chromatograms of the J_1b oils and potential source rocks (Fig. 7). The carbon number distribution of this series of compounds in both the oils and the source rocks from the study area ranges from C_{28} – C_{35} , with a maximum peak at C_{30} (Fig. 7). Abundant

gammacerane (G) is observed in the J_1b oils (Fig. 7a and b), and the G/C_{30} –H values range from 0.31 to 0.89 (Table 3). The P_2w source rock samples show a relatively lower gammacerane content than the J_1b oils (Fig. 7c), with a G/C_{30} –H ratio of 0.13 (Table 1). The P_{1f} source rocks are rich in gammacerane (Fig. 7d), with G/C_{30} –H ratios of 0.19–1.10 (Table 3). Gammacerane is usually regarded as an indicator of water stratification in a hypersaline environment (Ten Haven et al., 1989; Peters et al., 2005) since its biogenic precursor is tetrahymanol, which is biosynthesized by the abundant anaerobic ciliates that form under such conditions (Sinninghe, Damsté et al., 1995). The compound is abundant in saline lacustrine source rocks and hence in the sampled oils. This further supports the inference that the J_1b oils mainly originate from the P_{1f} source rocks rather than the P_2w source rocks.

Relatively high abundances of C_{35} -homohopanes (C_{35} –H) in

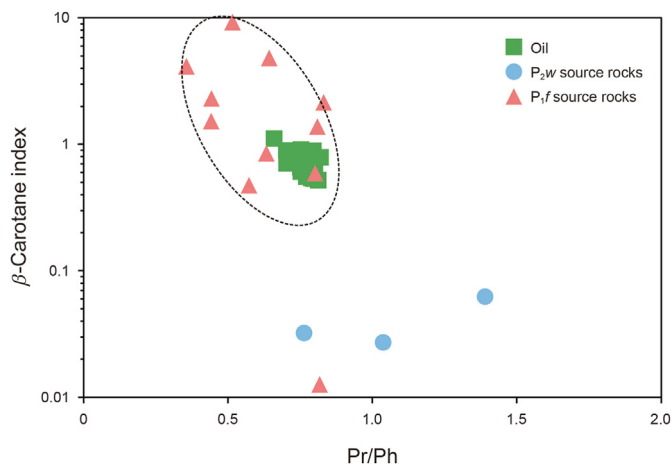


Fig. 6. Cross-plots of Pr/Ph and β -carotane index (β -carotane/ C_{max}).

both crude oils and source rock extracts are generally associated with organic matter deposited in a highly saline and strongly reducing water body, while low contents of these compounds indicate an oxidizing environment (Peters and Moldowan, 1991; Peters et al., 2005). In this study, the C_{35} –H contents of the J_1b oils are high (Fig. 7). As Fig. 7 shows, the homoeopathy series of compounds in all the J_1b oil samples exhibit a V-shape pattern, as illustrated by the distribution C_{31} –H > C_{32} –H > C_{33} –H > C_{34} –H < C_{35} –H. This is indicative of hypersaline lacustrine source rocks deposited under strongly reducing, high pH conditions (Peters and Moldowan, 1991; Peters et al., 2005). Unlike the J_1b oils, the P_{2w} source rocks contain little C_{35} –H, with a steady decrease in peak content with increasing carbon number (Fig. 7c), indicating that the organic matter may have formed under oxic conditions. The P_{1f} source rocks show the reverse, with all the P_{1f} source rock samples containing higher

C_{35} –H than the P_{2w} source rocks (Fig. 7d). P_{1f} must therefore have been deposited in a more reducing environment than P_{2w} . As shown in Fig. 8, the data from the J_1b oils are similar to those of the P_{1f} source rock samples, showing extreme affinity between the oils and the source rocks and indicating that these crude oils were mainly derived from the P_{1f} source rocks. This conclusion is also supported by the low Pr/Ph ratios and high β -carotane index (Fig. 6).

The ratios of C_{31} H–22 S/(S + R) in the oils range from 0.65 to 0.85 (Table 3), indicating that the oils have reached empirical thermal equilibrium and are mature crude oils.

4.3.4. Steranes

Fig. 9 shows the regular steranes distribution for typical oils and source rocks from the study area (Fig. 9). All oil samples from the area have essentially identical distributions, dominated by C_{29} regular steranes (Fig. 9a and b). The content of C_{27} steranes mostly ranges from 3.05 to 13.93%, with an average of 7.54% (Table 3). C_{29} steranes also predominate in the solvent extracts from the P_{2w} source rocks, but these contain commensurate amounts of C_{27} regular steranes (Fig. 9c). The contents of C_{27} steranes in the P_{2w} source rocks range between 31.19 and 38.72%, higher than those of the oils (Table 3). The solvent extracts from the P_{1f} source rocks contain much higher amounts of C_{29} steranes than C_{27} and C_{28} steranes (Fig. 9d). The distribution of C_{27} steranes ratios for the P_{1f} source rocks is similar to that of the oils, ranging from 3.15 to 6.89% (Table 3).

The relative proportions of C_{27} , C_{28} and C_{29} regular steranes in source rock extracts can be used as a correlation parameter to ascertain the organic matter type and the sedimentary environment, because the ratio generally remains constant throughout the thermal generation of oil (Huang and Meinschein, 1979; Peters et al., 2005). The ternary diagram in Fig. 10a shows the relative proportions of C_{27} – C_{29} regular steranes in the oils and source rocks from the study area. The steranes compositions of all the oil

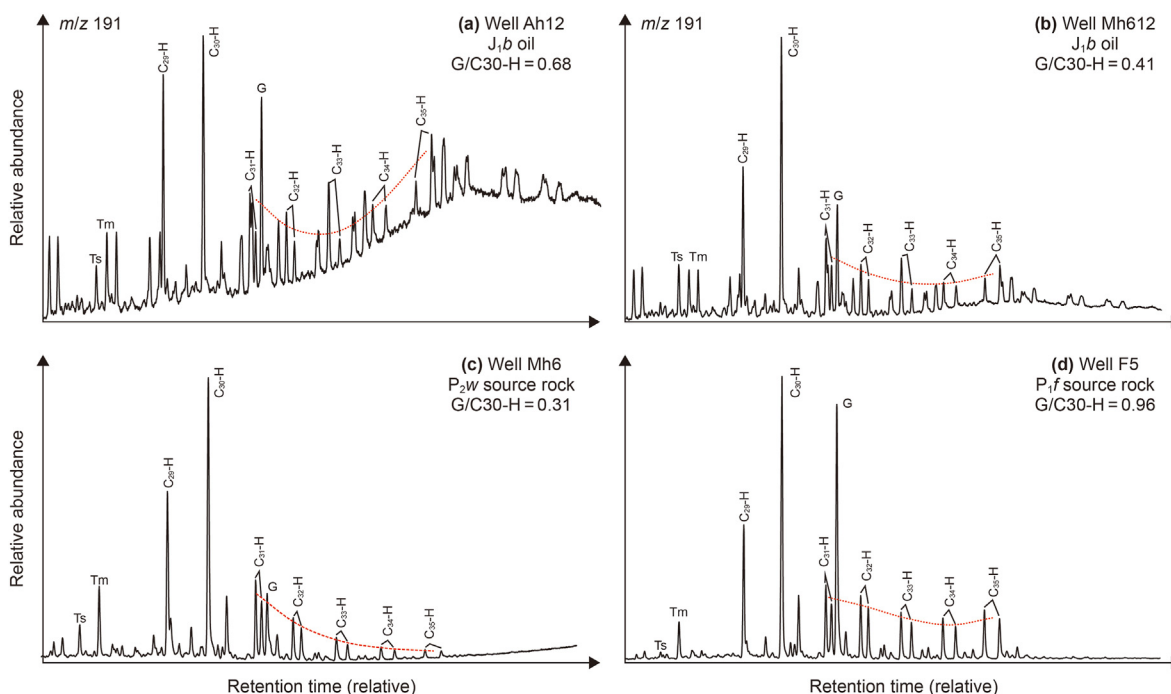


Fig. 7. Representative m/z 191 fragmentograms of the saturated fraction showing the distribution of terpane for (a) and (b) the J_1b oils, (c) solvent extracts of P_{2w} source rocks, and (d) solvent extracts of P_{1f} source rocks.

Table 3

Parameters of hopanes and steranes from source rock extracts and oils in the study area.

Sample ID	G/C ₃₀ -H	C ₃₁ -H S/(S + R)	C ₃₁ -H, %	C ₃₂ -H, %	C ₃₃ -H, %	C ₃₄ -H, %	C ₃₅ -H, %	C ₂₇ -St, %	C ₂₈ -St, %	C ₂₉ -St, %	C ₂₉ -St $\beta\beta/(\beta\beta + \alpha\alpha)$	C ₂₉ -St S/(S + R)
F1	1.10	0.59	0.27	0.23	0.16	0.16	0.18	6.33	9.28	58.48	0.20	0.35
F2	1.06	0.59	0.28	0.23	0.16	0.16	0.17	6.89	32.20	36.61	0.19	0.35
F3	0.96	0.56	0.25	0.23	0.17	0.16	0.20	6.66	29.77	31.51	0.21	0.36
F4	0.35	0.55	0.38	0.22	0.15	0.12	0.14	3.40	47.35	46.32	0.33	0.42
F5	0.47	0.58	0.39	0.24	0.15	0.11	0.10	5.56	47.20	45.91	0.37	0.46
F6	0.34	0.55	0.42	0.28	0.14	0.10	0.07	3.15	48.66	44.69	0.26	0.32
F7	0.68	0.60	0.34	0.23	0.16	0.13	0.14	5.71	43.34	53.26	0.20	0.30
F8	0.64	0.64	0.30	0.21	0.17	0.14	0.18	6.46	46.07	48.36	0.25	0.36
F9	0.27	0.55	0.46	0.25	0.13	0.08	0.07	5.37	44.40	52.45	0.42	0.47
F10	0.19	0.55	0.45	0.26	0.14	0.09	0.07	5.91	44.87	49.42	0.41	0.46
F11	0.17	0.54	0.42	0.29	0.15	0.08	0.06	31.83	43.66	49.88	0.39	0.44
W1	0.03	0.59	0.46	0.29	0.13	0.09	0.04	32.24	47.91	46.73	0.29	0.42
W2	0.21	0.55	0.43	0.26	0.15	0.09	0.07	31.19	43.72	50.37	0.34	0.41
W3	0.15	0.54	0.42	0.27	0.16	0.09	0.05	38.72	32.26	35.92	0.38	0.43
M1	0.64	0.78	0.26	0.12	0.16	0.16	0.30	16.93	41.73	41.34	0.62	0.50
M2	0.51	0.75	0.29	0.15	0.16	0.15	0.25	3.66	47.04	49.30	0.59	0.50
M3	0.53	0.79	0.30	0.15	0.17	0.15	0.23	3.99	46.03	49.98	0.60	0.50
M4	0.51	0.77	0.30	0.16	0.16	0.11	0.26	13.00	41.90	45.10	0.60	0.49
M5	0.54	0.77	0.29	0.15	0.17	0.11	0.28	4.16	46.84	49.00	0.60	0.49
M6	0.41	0.73	0.30	0.15	0.18	0.13	0.24	3.77	47.83	48.41	0.58	0.49
M7	0.79	0.79	0.26	0.12	0.16	0.15	0.31	13.54	38.94	47.52	0.63	0.51
M8	0.66	0.80	0.27	0.14	0.18	0.11	0.30	7.15	43.50	49.35	0.62	0.49
M9	0.40	0.72	0.31	0.17	0.18	0.11	0.23	5.49	46.79	47.72	0.56	0.49
M10	0.58	0.78	0.29	0.14	0.16	0.15	0.26	13.61	43.57	42.82	0.60	0.50
M11	0.67	0.79	0.29	0.14	0.17	0.09	0.31	6.68	47.68	45.64	0.63	0.50
M12	0.65	0.79	0.31	0.14	0.17	0.10	0.29	9.23	44.04	46.73	0.63	0.50
M13	0.72	0.80	0.30	0.14	0.18	0.10	0.29	7.14	44.47	48.39	0.63	0.50
M14	0.68	0.76	0.29	0.14	0.17	0.11	0.29	17.59	40.77	41.65	0.63	0.50
M15	0.41	0.73	0.31	0.17	0.18	0.12	0.23	4.30	45.99	49.71	0.56	0.49
M16	0.72	0.80	0.25	0.11	0.17	0.17	0.30	6.46	45.78	47.76	0.62	0.50
M17	0.71	0.78	0.30	0.15	0.17	0.10	0.29	7.13	44.01	48.86	0.62	0.51
M18	0.75	0.78	0.29	0.14	0.17	0.09	0.30	6.70	43.56	49.74	0.63	0.50
M19	0.64	0.78	0.30	0.15	0.17	0.11	0.27	8.99	44.13	46.88	0.63	0.50
M20	0.41	0.73	0.32	0.16	0.18	0.11	0.23	7.22	43.74	49.03	0.56	0.49
M21	0.59	0.76	0.28	0.13	0.17	0.12	0.30	10.73	41.44	47.83	0.61	0.50
M22	0.65	0.77	0.29	0.13	0.16	0.11	0.30	7.69	43.41	48.90	0.62	0.50
M23	0.57	0.80	0.32	0.14	0.16	0.11	0.27	6.71	46.02	47.28	0.60	0.51
M24	0.66	0.80	0.29	0.14	0.17	0.10	0.29	5.73	46.78	47.49	0.62	0.50
M25	0.89	0.78	0.32	0.15	0.17	0.10	0.26	6.15	45.97	47.88	0.63	0.50
M26	0.75	0.78	0.31	0.14	0.17	0.12	0.26	5.63	43.35	51.02	0.63	0.50
M27	0.79	0.77	0.30	0.14	0.18	0.11	0.27	10.17	44.43	45.41	0.63	0.51
M28	0.74	0.77	0.33	0.13	0.16	0.09	0.29	4.85	44.61	50.55	0.63	0.50
M29	0.71	0.77	0.30	0.14	0.17	0.11	0.28	6.36	45.46	48.17	0.64	0.50
M30	0.66	0.76	0.30	0.13	0.18	0.09	0.29	8.94	45.90	45.16	0.62	0.51
M31	0.81	0.80	0.29	0.13	0.18	0.12	0.28	4.73	45.41	49.86	0.64	0.50
M32	0.85	0.79	0.31	0.13	0.17	0.11	0.28	5.71	45.31	48.97	0.64	0.50
M33	0.46	0.74	0.34	0.16	0.16	0.09	0.25	7.51	43.74	48.75	0.62	0.49
M34	0.71	0.79	0.30	0.13	0.18	0.09	0.29	12.30	40.70	47.00	0.64	0.50
M35	0.81	0.78	0.32	0.13	0.16	0.10	0.29	8.15	44.58	47.27	0.64	0.50
M36	0.49	0.75	0.30	0.16	0.17	0.12	0.25	3.05	45.82	51.13	0.60	0.50
M37	0.76	0.79	0.28	0.13	0.17	0.17	0.26	7.82	44.49	47.69	0.63	0.50
M38	0.78	0.77	0.30	0.13	0.17	0.12	0.29	4.78	47.29	47.93	0.63	0.51
M39	0.70	0.77	0.31	0.13	0.17	0.11	0.27	6.44	45.60	47.96	0.61	0.51
I1	0.51	0.74	0.27	0.14	0.15	0.17	0.28	7.36	43.52	49.11	0.61	0.49
I2	0.40	0.71	0.29	0.16	0.18	0.11	0.27	4.56	46.15	49.28	0.55	0.48
I3	0.68	0.76	0.27	0.13	0.18	0.09	0.33	5.50	44.67	49.83	0.47	0.54
I4	0.31	0.70	0.34	0.16	0.18	0.10	0.22	6.84	47.40	45.75	0.55	0.48
I5	0.73	0.82	0.27	0.12	0.17	0.13	0.31	7.26	45.16	47.58	0.56	0.49

Notes: G/C₃₀-H: Gammacerane/C₃₀-Hopane; C₃₁-H S/(S + R): C₃₁-Hopane 22 S/(22 S + 22 R); C₃₁-H(%): C₃₁-Hopane/C₃₁-C₃₅-Hopane; C₃₂-H(%): C₃₂-Hopane/C₃₁-C₃₅-Hopane; C₃₃-H(%): C₃₃-Hopane/C₃₁-C₃₅-Hopane; C₃₄-H(%): C₃₄-Hopane/C₃₁-C₃₅-Hopane; C₃₅-H(%): C₃₅-Hopane/C₃₁-C₃₅-Hopane; C₂₇-St(%): C₂₇ regular sterane/C₂₇-C₂₉ regular steranes; C₂₈-St(%): C₂₈ regular sterane/C₂₇-C₂₉ regular steranes; C₂₉-St(%): C₂₉ regular sterane/C₂₇-C₂₉ regular steranes; C₂₉- $\beta\beta/(\beta\beta + \alpha\alpha)$: C₂₉-St $\alpha\beta\beta/C_{29}$ ($\alpha\beta\beta + \alpha\alpha\alpha$) regular steranes; C₂₉-St S/(S + R): C₂₉-20 S/C₂₉ (20 S + 20 R) regular sterane.

samples are consistent, clearly showing that the oils all belong to a single family and that their source affinities are similar. The data from the J₁b oils and P₁f extracts are plotted close together in one area of the ternary diagram, indicating that those oils were mainly sourced from the P₁f source rocks.

Generally, C₂₇ regular steranes originate from aquatic organisms, while C₂₉ regular steranes typically originate from higher plants. However, C₂₉ regular steranes may also be derived from

some special marine organisms. For example, in the Permit Basin, the organic matter in the Cretaceous source rocks is mainly derived from algae, but the distribution of regular steranes is dominated by C₂₉ steranes (Wan et al., 2014). C₂₉ steranes also predominate in Cambrian source rocks in the Tarim Basin (Cai et al., 2009). Since terrestrial higher plants did not appear until after the Late Silurian (Banks, 1975), the high contents of C₂₉ steranes that are found in sediments deposited prior to the Late Silurian must be related to

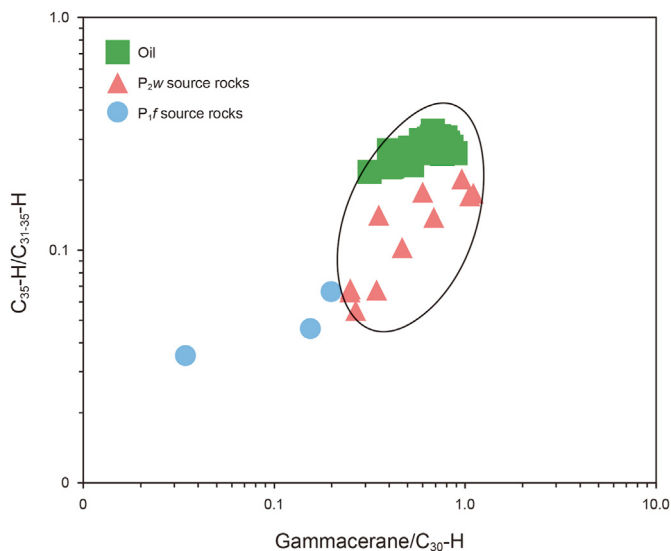


Fig. 8. Cross plot of gammacerane/ C_{30} -H ratios and C_{35} -H relative content.

marine organic matter. Green algae of the class Prasinophyceae have been considered to be the likely biological sources of C_{29} steranes prior to the appearance of higher plants (Volkman et al., 1994). In this study, the distributions of n -alkanes, acyclic isoprenoids, and hopanes indicate that the organic matter in the P_{1f} source rocks is mainly derived from aquatic organisms. Petrographic observations also indicate a predominantly marine organic matter composition for the P_{1f} source rocks in the Mahu Sag (Xiao et al., 2021; Hou et al., 2022). The C_{29} regular sterane composition is therefore likely to represent some special marine organic matter, such as photosynthetic planktonic or green algae (Volkman, 1988; Peters et al., 2005; Liu et al., 2022). However, the origins of C_{29} regular steranes in the P_{2w} and in the P_{1f} source rocks may be completely different. The distribution of regular steranes in the J_1b oils shows compositional similarity with the P_{1f} source rocks (Fig. 9), further indicating that the J_1b oils originate from the P_{1f} source rocks.

The ratios of $C_{29}\alpha\beta\beta/(\alpha\beta\beta + \alpha\alpha\alpha)$ and $C_{29}20\text{ S}/(20\text{ S} + 20\text{ R})$ regular steranes in oils range from 0.55 to 0.64 and 0.48 to 0.54 (Table 3), both reaching empirical thermal equilibrium values, which indicates mature crude oils (Peters et al., 2005).

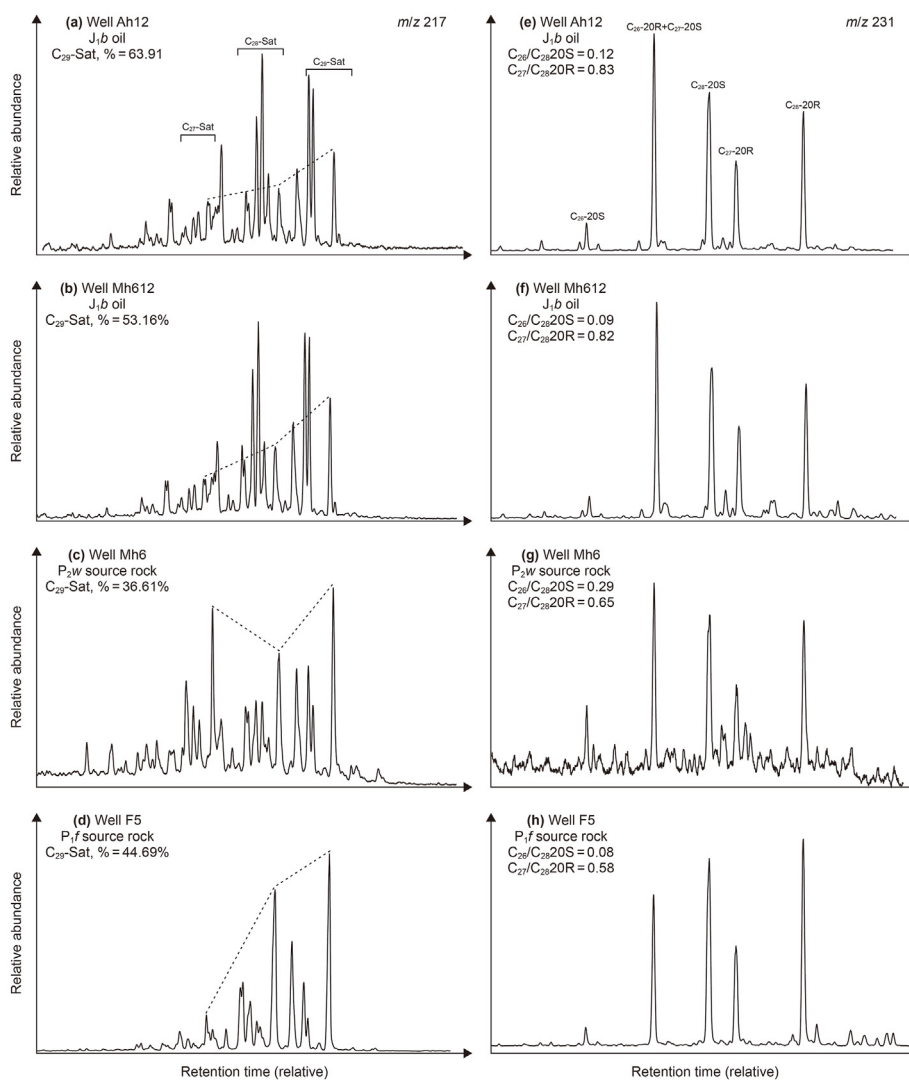


Fig. 9. (a–d) Representative m/z 217 fragmentograms of saturated fractions showing the distribution of steranes and (e–h) representative m/z 231 fragmentograms of aromatic fractions showing the distribution of TAS.

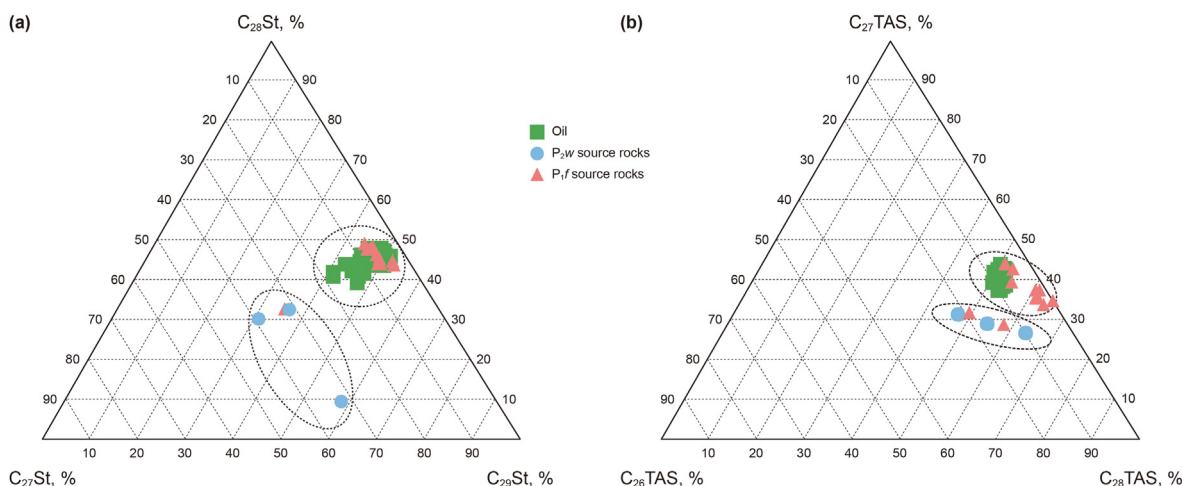


Fig. 10. Ternary diagram showing the relative abundances of: (a) C_{27} , C_{28} and C_{29} regular steranes, and (b) C_{26} , C_{27} and C_{28} TAS in the J_1b oil and Permian source rocks from the study area.

4.3.5. Triaromatic steroids (TAS)

The distributions of TAS in the J_1b oils and the solvent extracts from the source rocks are shown in Fig. 9. By comparison of relative retention times with the literature, all TAS isomers in the m/z 231 mass chromatogram of aromatic fractions can be positively identified (Fig. 9). The C_{28} –20 S TAS, C_{27} –20 R TAS, and C_{28} –20 R TAS predominate and are distinctly more abundant than C_{26} –20 S TAS in the oils (Fig. 9e and f). The distributions of TAS in the solvent extracts from the P_{1f} source rocks are characterized by low concentrations of C_{26} –20 S TAS, similar to the oils (Fig. 9h). However, the C_{26} –20 S TAS contents in solvent extracts from the P_{2w} source rocks are significantly higher than those in the J_1b oils and P_{1f} source rocks (Fig. 9g) with particularly high C_{26}/C_{28} –20 S TAS ratios (Table 4). The C_{26}/C_{28} –20 S TAS ratios in the J_1b oils are extremely low (Table 4), comparable to the ratios for the solvent extracts from the P_{1f} source rocks. This result again tends to confirm that all the oils derive from the P_{1f} source rocks.

The relative contents of C_{26} –TAS, C_{27} –TAS, and C_{28} –TAS cannot be determined from routine m/z 231 mass chromatograms of aromatic fractions, due to the co-occurrence of C_{26} –20 S TAS and C_{27} –20 R TAS (Peters et al., 2005; Killips et al., 2021) (Fig. 10a). However, Zhang et al. (2016) proposed that the contents of C_{26} –20 R TAS and C_{27} –20 S TAS can be respectively estimated by calculating the relative contents of C_{28} –20 S TAS and C_{28} –20 R TAS, since the isomers of C_{28} TAS can be unequivocally identified. This process has been successfully applied for oil group division and oil-source correlation in the Tarim and Beibu Gulf Basins (Yang et al., 2015, 2017; Zhang et al., 2016). In this study, a ternary diagram of C_{26} –TAS, C_{27} –TAS and C_{28} –TAS for the J_1b oils and the solvent extracts from the source rocks was established using this method for oil-source rock correlation (Fig. 10b). The contents of C_{26} –20 S TAS in the P_{1f} source rocks and the oil samples are distinctly low, suggesting that the oil samples are clustered with the P_{1f} source rocks. However, the content of C_{26} TAS in the P_{2w} source rocks is markedly higher, ranging from 10% to 22% (Table 4). These results further confirm that the crude oils derive from the P_{1f} source rocks.

4.3.6. Stable carbon isotope evidences

Chen et al. (2016) reported that the organic matter of P_{2w} source rocks is rich in the heavy carbon isotope, with $\delta^{13}C$ values ranging from -23.00‰ to -21.00‰ , indicating the dominant input of terrestrial plants. However, the organic matter of P_{1f} source rocks is

rich in light carbon isotope, with $\delta^{13}C$ values ranging from -31.50‰ to -26.00‰ , showing a predominant input of aquatic organisms. In this study, the $\delta^{13}C$ values of P_{2w} source rocks is distinctly higher than those of P_{1f} source rocks. The $\delta^{13}C$ values of J_1b oils are within the range of -28.64‰ to -29.54‰ (Table 4), which is consistent with those of P_{1f} source rocks. Therefore, it is conceivable that J_1b oils were derived from P_{1f} source rocks rather than P_{2w} source rocks (Wang et al., 2022).

4.4. Petroleum accumulation process

Based on the hydrocarbon generation and expulsion history of source rocks in the study area, two oil filling events took place for J_1b reservoirs i.e. Late Jurassic–Early Cretaceous and Paleogene–Neogene, respectively (Zhi et al., 2021).

Feng et al. (2019) reported that two major hydrocarbon generation and expulsion events for P_{1f} source rock occurred on the basis of the thermal evolution history and burial history. The estimated timing for hydrocarbon generation of P_{1f} source rock are Early Triassic for the first stage and Early Jurassic for the second one. Moreover, the Late Triassic–Early Jurassic and Late Jurassic–Early Cretaceous are the main times for hydrocarbon expulsion for P_{1f} source rock.

The basin modeling indicates that the source rocks entered the oil window in Early Triassic (Fig. 11a), and oil generation for the first stage began (Feng et al., 2019). However, there were no large-scale oil and gas accumulation due to the lack of effective traps. The second hydrocarbon generation process for P_{1f} source rock took place in the Late Triassic through Early Jurassic. The generated petroleum migrated and accumulated in the Early Triassic (T_1b glutenite) reservoirs (Fig. 11b). The migration pathways are mainly faults and reservoir rocks with good permeability (Feng et al., 2019).

During the Late Jurassic–Early Cretaceous, it is the critical time for the second stage of petroleum expulsion from P_{1f} source rock, resulting in the oil pools formed in the T_1b glutenite reservoirs (Fig. 11c). At this time, the Jurassic reservoirs began to form. The Dazhuluogou Faults formed during this period and cut from P_{1f} source rock to Jurassic reservoirs (Bian et al., 2019; Wu et al., 2014), which provided the vertical migration pathways of petroleum leading to the formation of oil pools in the Well Mh1 block (Fig. 11e). Meanwhile, some new secondary faults developed in

Table 4

Parameters of triaromatic steroids form source rock extracts and oils in the study area.

Sample ID	C ₂₆ –/C ₂₈ –20 S	C ₂₇ –/C ₂₈ –20 R	C ₂₆ TAS, %	C ₂₇ TAS, %	C ₂₈ TAS, %	δ ¹³ C, ‰
F1	0.06	0.54	0.02	0.34	0.64	–29.52
F2	0.08	0.63	0.02	0.38	0.60	–28.25
F3	0.08	0.59	0.03	0.36	0.61	nd
F4	0.09	0.82	0.04	0.43	0.53	–29.25
F5	0.11	0.88	0.05	0.45	0.51	–28.83
F6	0.03	0.54	0.00	0.35	0.65	–30.47
F7	0.07	0.58	0.03	0.36	0.62	nd
F8	0.05	0.62	0.01	0.38	0.61	nd
F9	0.07	0.74	0.06	0.40	0.54	–28.40
F10	0.34	0.66	0.19	0.32	0.49	–26.13
F11	0.22	0.51	0.13	0.29	0.58	nd
W1	0.16	0.43	0.10	0.27	0.63	–23.02
W2	0.29	0.55	0.17	0.30	0.54	–22.54
W3	0.43	0.69	0.22	0.32	0.46	nd
M1	0.10	0.79	0.08	0.41	0.52	–28.64
M2	0.10	0.80	0.09	0.40	0.51	nd
M3	0.09	0.78	0.09	0.40	0.51	nd
M4	0.09	0.83	0.07	0.42	0.51	nd
M5	0.10	0.81	0.07	0.41	0.51	nd
M6	0.10	0.90	0.06	0.45	0.49	nd
M7	0.09	0.76	0.08	0.40	0.52	nd
M8	0.09	0.74	0.09	0.38	0.52	nd
M9	0.09	0.83	0.07	0.42	0.51	nd
M10	0.09	0.81	0.07	0.41	0.52	nd
M11	0.09	0.75	0.08	0.39	0.52	nd
M12	0.11	0.82	0.08	0.41	0.50	nd
M13	0.10	0.78	0.08	0.40	0.52	nd
M14	0.10	0.78	0.08	0.40	0.51	nd
M15	0.11	0.87	0.06	0.44	0.51	nd
M16	0.10	0.80	0.09	0.41	0.51	nd
M17	0.10	0.79	0.08	0.40	0.51	nd
M18	0.09	0.78	0.08	0.40	0.52	nd
M19	0.10	0.80	0.08	0.41	0.51	nd
M20	0.09	0.82	0.07	0.42	0.51	–29.54
M21	0.11	0.83	0.08	0.42	0.50	nd
M22	0.11	0.82	0.08	0.42	0.51	nd
M23	0.12	0.86	0.08	0.43	0.50	nd
M24	0.10	0.78	0.08	0.40	0.52	nd
M25	0.09	0.74	0.08	0.39	0.53	nd
M26	0.09	0.75	0.09	0.39	0.52	nd
M27	0.10	0.79	0.08	0.40	0.51	nd
M28	0.10	0.79	0.08	0.40	0.51	nd
M29	0.11	0.80	0.10	0.40	0.50	nd
M30	0.10	0.80	0.10	0.40	0.50	nd
M31	0.09	0.75	0.09	0.39	0.52	nd
M32	0.09	0.72	0.10	0.38	0.52	nd
M33	0.09	0.75	0.09	0.39	0.52	nd
M34	0.09	0.73	0.10	0.38	0.52	nd
M35	0.09	0.73	0.09	0.38	0.52	nd
M36	0.12	0.88	0.08	0.43	0.49	nd
M37	0.09	0.77	0.08	0.40	0.52	nd
M38	0.10	0.79	0.08	0.40	0.51	nd
M39	0.10	0.79	0.08	0.41	0.51	nd
I1	0.09	0.79	0.07	0.41	0.52	nd
I2	0.11	0.85	0.06	0.43	0.51	nd
I3	0.12	0.83	0.08	0.41	0.50	–28.73
I4	0.13	0.84	0.06	0.43	0.51	nd
I5	0.14	0.87	0.09	0.43	0.49	nd

Notes: C₂₆–/C₂₈–20 S: C₂₆–20 S/C₂₈–20STAS; C₂₇–/C₂₈–20 R: C₂₇–20 R/C₂₈–20RTAS; C₂₆ TAS(%): C₂₆TAS/(C₂₆ + C₂₇ + C₂₈)TAS; C₂₇TAS(%): C₂₇TAS/(C₂₆ + C₂₇ + C₂₈) TAS; C₂₈TAS(%): C₂₈TAS/(C₂₆ + C₂₇ + C₂₈) TAS; δ¹³C: carbon isotope for kerogen of source rock, carbon isotope for whole oil; nd: no data.

Jurassic though Triassic, resulting in the migration of Triassic oils via those faults and the accumulation of J_{1b} reservoirs (Fig. 11f), which could be confirmed by a high degree of similarity of Jurassic and Triassic oils in molecular compositions (Hu et al., 2020). In the Paleogene–Neogene, normal faults of shallow strata cutting from Triassic to Jurassic were remobilized (Zhi et al., 2021), leading to the leakage of Triassic oil to the J_{1b} reservoirs (Fig. 11e and f). Thus, the faults with different buried depths serve as favorable conduits for the oil migration and accumulation of J_{1b} oil pools in the Mahu Sag.

4.5. Exploration potential for shallow reservoirs

The analyzed oil samples in this study belong to the same oil group and were derived from P_{1f} source rocks. In the study area, the core from the P_{1f} source rock bed contain substantial amounts of oil-prone organic matter that have reached mature to high mature stage, suggesting active generation of hydrocarbons in the shallow strata. The thrust faults and shallow-buried secondary faults were important factors in conducting petroleum migration and accumulation of Jurassic reservoirs revealed by the basin modeling

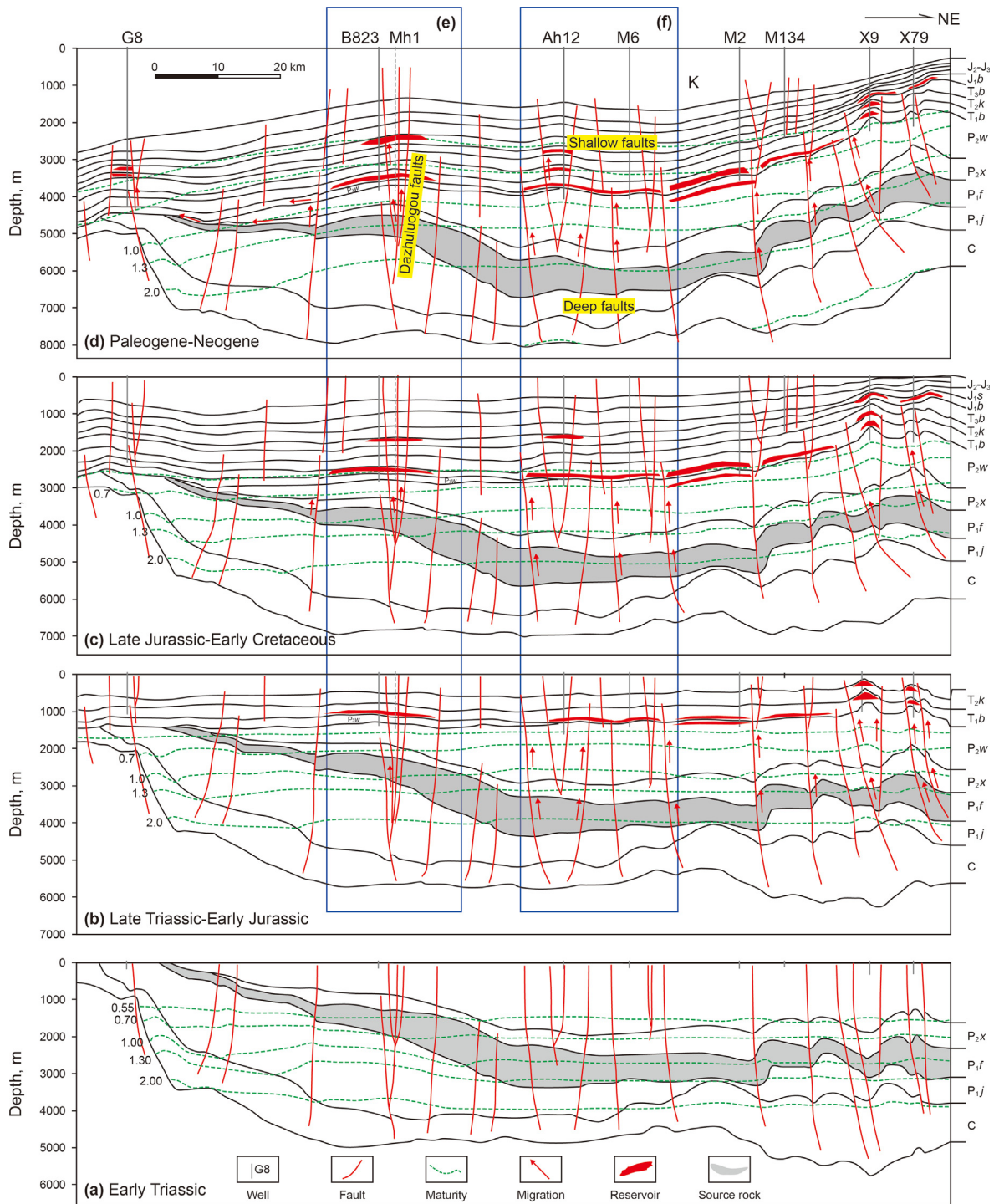


Fig. 11. Two-dimensional (2D) basin modeling of hydrocarbon migrations and accumulations in geological history, the location of section is shown in Fig. 1b.

analysis. The mudstone of J_{1s}, J_{2t}, and K_{1tg} formed under lacustrine transgressive effectively prevented the leakage of J_{1b} oils (Qian et al., 2018). The commercial oil flow produced from J_{1b} reservoirs in wells AH12, M606, M612 and Mh1 shows an excellent exploration potential in this area (Hu et al., 2020). The highs connecting source rock beds and T_{1b} oil reservoirs by faults may be favorable exploration targets.

5. Conclusions

Geochemical investigation, including source rock, crude oil, and biomarker analysis, was performed on a major, but rarely studied, shallow-buried saline oil field in the Mahu Sag. Analysis of 44 oil samples from the Jurassic production fields in the Junggar basin revealed the presence of only one oil group, with all the crude oils exhibiting a high degree of similarity, pointing to a similar origin. These saline oils are characterized by: (1) low Pr/Ph (average 0.8),

(2) high abundance of β -carotane (average β -carotane index 2), (3) high contents of C_{35} -H and gammacerane, and (4) predominance of C_{29} regular sterane, suggesting that the source rocks were deposited in an anoxic environment with aquatic organism input.

Oil-source correlation indicates that the crude oils mostly originate from the P_1f source rocks, which are characterized by: (1) low Pr/Ph (average of 0.8), (2) high abundance of β -carotane (average β -carotane index of 4), (3) high content of C_{35} -H and gammacerane, and (4) high C_{29} regular sterane predominance, indicating that they formed in a highly saline and strongly reducing water body with contributions almost exclusively from aquatic organisms. The P_2w source rocks are characterized by: (1) low abundance of β -carotane (average β -carotane index of 0.1), (2) lower contents of C_{35} -H and gammacerane, and (3) higher C_{27} regular steranes, indicating an oxidizing environment with input from a mixture of aquatic organisms and terrigenous higher plants. These source rocks, however, make only a minor contribution to the crude oils. It is therefore concluded that the saline oils discovered in shallow strata in the western slope of the Mahu Sag mainly derive from the alkaline source rocks of the P_1f Formation.

2D basin modeling and numerical simulation were applied to reconstruct the maturity evolution of P_1f source rock and J_1b oil accumulation process. The results show that petroleum generation of P_1f started around the Early Triassic and the Early Jurassic. Twice significant oil filling for J_1b reservoirs took place in Late Jurassic–Early Cretaceous and Paleogene–Neogene. The oil filling pathways mainly are the trust faults cutting from the source beds to Jurassic and secondary faults with different buried depth. The major exploration targets in the future are the nose structures connecting P_1f source beds and T_1b oil reservoirs by faults.

Declaration of competing interest

The authors declare that they have no known competing financial interests or personal relationships that could have appeared to influence the work reported in this paper.

Acknowledgment

This work was supported by the National Natural Science Foundation of China (No. 41802179), Sichuan Science and Technology Program (No. 2019YFH0037) and the Foundation of the State Key Laboratory of Petroleum Resources and Prospecting, China University of Petroleum, Beijing (No. PRP/open-1906). The authors thank the Xinjiang Oil Field Company for providing the samples and surface maps used in this study and for permitting them to be published. We extend our thanks to Associate Editor and the anonymous reviewers for their constructive comments. We would particularly like to express our gratitude to Lei Zhu and Shengbao Shi for their generous assistance with the experiments.

References

- Abulimit, I., Tang, Y., Cao, J., Chen, G., Chen, J., Tao, K., 2016. Accumulation mechanism and controlling factors of the continuous hydrocarbon plays in the lower triassic Baikouquan Formation of the Mahu sag, Junggar Basin, China. *J. Nat. Gas. Geosci.* 1 (4), 309–318. <https://doi.org/10.1016/j.jnggs.2016.10.003>.
- Bian, B., Zhang, J., Wu, J., Li, Z., Wang, Y., Cao, J., 2019. Re-characterization of the Dazhuluogou strike-slip fault in northwestern Junggar Basin and the implications for hydrocarbon accumulation. *Earth Sci. Front.* 26 (1), 238–247. <https://doi.org/10.13745/j.esf.2019.1.14> (in Chinese).
- Banks, H.P., 1975. Early vascular land plants: proof and conjecture. *Bioscience* 25 (11), 730–737. <https://doi.org/10.2307/1297453>.
- Brooks, J.D., Gould, K., Smith, J.W., 1969. Isoprenoid hydrocarbons in coal and petroleum. *Nature* 222 (5190), 257–259. <https://doi.org/10.1038/22257a0>.
- Brooks, J.D., Smith, J.W., 1969. The diagenesis of plant lipids during the formation of coal, petroleum and natural gas—II. Coalification and the formation of oil and gas in the Gippsland Basin. *Geochem. Cosmochim. Acta* 33 (10), 1183–1194. [https://doi.org/10.1016/0016-7037\(69\)90040-4](https://doi.org/10.1016/0016-7037(69)90040-4).
- Cao, J., Zhang, Y., Hu, W., Yao, S., Wang, X., Zhang, Y., Tang, Y., 2005. The Permian hybrid petroleum system in the northwest margin of the Junggar Basin, northwest China. *Mar. Petrol. Geol.* 22 (3), 331–349. <https://doi.org/10.1016/j.marpetgeo.2005.01.005>.
- Cao, J., Lei, D., Li, Y., Tang, Y., Imin, A., Chang, Q., Wang, T., et al., 2015. Ancient high-quality alkaline lacustrine source rocks discovered in the lower permian Fengcheng Formation, Junggar Basin. *Acta Petrol. Sin.* 36 (7), 781–790. <https://doi.org/10.7623/syxb201507002> (in Chinese).
- Cao, J., Xia, L., Wang, T., Zhi, D., Tang, Y., Li, W., 2020. An alkaline lake in the Late Paleozoic Ice Age (LPIA): a review and new insights into paleoenvironment and petroleum geology. *Earth Sci. Rev.* 202, 103091. <https://doi.org/10.1016/j.earscirev.2020.103091>.
- Cai, C., Li, K., Anlai, M., Zhang, C., Xu, Z., Worden, R.H., Wu, G., Zhang, B., Chen, L., 2009. Distinguishing cambrian from upper ordovician source rocks: evidence from sulfur isotopes and biomarkers in the Tarim Basin. *Org. Geochem.* 40 (7), 755–768. <https://doi.org/10.1016/j.orggeochem.2009.04.008>.
- Cai, H., Jin, J., Li, E., Zhang, Z., Gu, Y., Wang, Y., Yu, S., Pan, C., 2023. Unraveling gas charging and leakage for oil reservoirs in the Mahu sag of the Junggar Basin, NW China using concentrations and ratios of biomarkers, light hydrocarbons and diamondoids. *Org. Geochem.* 177, 104543. <https://doi.org/10.1016/j.orggeochem.2022.104543>.
- Chen, J., Wang, X., Deng, C., Liang, D., Zhang, Y., Zhao, Z., Ni, Y., Zhi, D., Yang, H., Wang, Y., 2016. Geochemical features of source rocks and crude oil in the Junggar Basin, Northwest China. *Acta Geol. Sin.* 90 (3), 37–67. <https://doi.org/10.19762/j.cnki.dizhixuebao.2016103> (in Chinese).
- Chen, L., Yang, Y., Wang, F., Lu, H., Zhang, Y., Wang, X., Li, Y., Li, C., 2020. Exploration history and enlightenment in Junggar Basin. *Xinjing Pet. Geol.* 41 (5), 505–518. <https://doi.org/10.7657/JPG20200501> (in Chinese).
- Chen, Y., Cheng, X., Zhang, H., Li, C., Ma, Y., Wang, G., 2018. Fault characteristics and control on hydrocarbon accumulation of middle-shallow layers in the slope zone of Mahu sag, Junggar Basin, NW China. *Petrol. Explor. Dev.* 45 (6), 1050–1060. [https://doi.org/10.1016/S1876-3804\(18\)30108-3](https://doi.org/10.1016/S1876-3804(18)30108-3).
- Chen, Z., Liu, G., Wang, X., Gao, G., Xiang, B., Ren, J., Ma, W., Zhang, Q., 2016. Origin and mixing of crude oils in Triassic reservoirs of Mahu slope area in Junggar Basin, NW China: implication for control on oil distribution in basin having multiple source rocks. *Mar. Petrol. Geol.* 78, 373–389. <https://doi.org/10.1016/j.marpetgeo.2016.09.022>.
- Chen, Z., Liu, G., Wang, X., Ren, J., Gao, G., Ma, W., Gao, P., 2017. Application of trace elements in mixed-oils classification and oil-source correlation. *J. China Univ. Petrol. Nat. Sci.* 41 (6), 50–63. <https://doi.org/10.3969/j.issn.1673-5005.2017.06.006> (in Chinese).
- Damsté, J.S.S., Kenig, F., Koopmans, M.P., et al., 1995. Evidence for gammacerane as an indicator of water column stratification. *Geochem. Cosmochim. Acta* 59 (9), 1895–1900. [https://doi.org/10.1016/0016-7037\(95\)00073-9](https://doi.org/10.1016/0016-7037(95)00073-9).
- Ding, W., Hou, D., Jiang, L., Jiang, Y., Wu, P., 2020. High abundance of carotanes in the brackish-saline lacustrine sediments: a possible cyanobacteria source? *Int. J. Coal Geol.* 219, 103373. <https://doi.org/10.1016/j.coal.2019.103373>.
- Ding, X., Gao, C., Zha, M., Chen, H., Su, Y., 2017. Depositional environment and factors controlling β -carotane accumulation: a case study from the Jimsar Sag, Junggar Basin, northwestern China. *Palaeogeogr. Palaeoclimatol. Palaeoecol.* 485, 833–842. <https://doi.org/10.1016/j.palaeo.2017.07.040>.
- Espitalié, J., Deroo, G., Marquis, F., 1985a. La pyrolyse Rock-Eval et ses applications. Deuxième partie. *Rev. Inst. Fr. Petrol.* 40 (6), 755–784. <https://doi.org/10.2516/ogst:1985045>.
- Espitalié, J., Deroo, G., Marquis, F., 1985b. Rock-Eval pyrolysis and its applications (part one). *Oil Gas Sci. Technol.* 40 (5), 563–579. <https://doi.org/10.2516/ogst:1985035>.
- Feng, C., Lei, D., Qu, J., Huo, J., 2019. Controls of paleo-overpressure, faults and sedimentary facies on the distribution of the high pressure and high production oil pools in the lower Triassic Baikouquan Formation of the Mahu Sag, Junggar Basin, China. *J. Petrol. Sci. Eng.* 176, 232–248. <https://doi.org/10.1016/j.petrol.2019.01.012>.
- Feng, C., Li, T., He, W., Zheng, M., 2020. Organic geochemical traits and paleo-depositional conditions of source rocks from the carboniferous to permian sediments of the northern Mahu sag, Junggar Basin, China. *J. Petrol. Sci. Eng.* 191, 107117. <https://doi.org/10.1016/j.petrol.2020.107117>.
- Gao, G., Yang, S., Ren, J., Zhang, W., Xiang, B., 2018. Geochemistry and depositional conditions of the carbonate-bearing lacustrine source rocks: a case study from the Early Permian Fengcheng Formation of Well FN7 in the northwestern Junggar Basin. *J. Petrol. Sci. Eng.* 162, 407–418. <https://doi.org/10.1016/j.petrol.2017.12.065>.
- Grba, N., Šajnović, A., Stojanović, K., Simić, V., Jovančević, B., Roglić, G., Erić, V., 2014. Preservation of diagenetic products of β -carotene in sedimentary rocks from the Lopare Basin (Bosnia and Herzegovina). *Geochem. (Tokyo)* 74 (1), 107–123. <https://doi.org/10.1016/j.jchemer.2013.10.002>.
- Hackley, P.C., Parris, T.M., Eble, C.F., Greb, S.F., Harris, D.C., 2021. Oil–source correlation studies in the shallow Berea Sandstone petroleum system, eastern Kentucky. *AAPG Bull.* 105 (3), 517–542. <https://doi.org/10.1306/08192019077>.
- He, D., Chen, X., Kuang, J., Yuan, H., Fan, C., Tang, Y., 2010. Distribution of Carboniferous source rocks and petroleum systems in the Junggar Basin. *Petrol. Explor. Dev.* 37 (4), 397–408. [https://doi.org/10.1016/S1876-3804\(10\)60041-9](https://doi.org/10.1016/S1876-3804(10)60041-9).
- He, D., Zhang, L., Wu, S., Li, D., Yu, Z., 2018. Tectonic evolution stages and features of the Junggar Basin. *Oil Gas Geol.* 39 (5), 845–861. <https://doi.org/10.11743/ogg20180501> (in Chinese).

- Hopmans, E.C., Schouten, S., Rijpstra, W.I.C., Damsté, J.S.S., 2005. Identification of carotenals in sediments. *Org. Geochem.* 36 (3), 485–495. <https://doi.org/10.1016/j.orggeochem.2004.10.001>.
- Hou, M., Qiu, J., Zha, M., Swennen, R., Ding, X., Imin, A., Liu, H., Bian, B., 2022. Significant contribution of haloalkaliphilic cyanobacteria to organic matter in an ancient alkaline lacustrine source rock: a case study from the Permian Fengcheng Formation, Junggar Basin, China. *Mar. Petrol. Geol.* 138, 105546. <https://doi.org/10.1016/j.marpetgeo.2022.105546>.
- Hu, X., Qu, Y., Hu, S., Pan, J., Yin, L., Xu, D., Teng, T., Wang, B., 2020. Geological conditions and exploration potential of shallow oil and gas in slope area of Mahu Sag, Junggar Basin. *Lithol. Reserv.* 32 (2), 67–77. <https://doi.org/10.12108/jxyq.20200207> (in Chinese).
- Huang, W., Meinschein, W.G., 1979. Sterols as ecological indicators. *Geochem. Cosmochim. Acta* 43 (5), 739–745. [https://doi.org/10.1016/0016-7037\(79\)90257-6](https://doi.org/10.1016/0016-7037(79)90257-6).
- Jia, H., Ji, H., Wang, L., Gao, Y., Li, X., Zhou, H., 2017. Reservoir quality variations within a conglomeratic fan-delta system in the Mahu sag, northwestern Junggar Basin: characteristics and controlling factors. *J. Petrol. Sci. Eng.* 152, 165–181. <https://doi.org/10.1016/j.petrol.2017.03.002>.
- Killops, S.D., Zhang, S., Lichtfouse, E., 2021. Triaromatic dinosteroids—Isomeric distributions and their geochemical significance. *Org. Geochem.* 162, 104300. <https://doi.org/10.1016/j.orggeochem.2021.104300>.
- Li, D., He, D., Santosh, M., Ma, D., 2015. Tectonic framework of the northern Junggar Basin Part II: the island arc basin system of the western Luliang Uplift and its link with the West Junggar terrane. *Gondwana Res.* 27 (3), 1110–1130. <https://doi.org/10.1016/j.gr.2014.08.019>.
- Li, D., He, D., Sun, M., Zhang, L., 2020. The role of arc-arc collision in accretionary orogenesis: insights from 320 Ma tectono-sedimentary transition in the kar-amaili area, NW China. *Tectonics* 39 (1), e2019T-e5623T. <https://doi.org/10.1029/2019TC005623>.
- Li, D., He, D., Tang, Y., 2016. Reconstructing multiple arc-basin systems in the altai-junggar area (NW China): implications for the architecture and evolution of the western central asian orogenic belt. *J. Asian Earth Sci.* 121, 84–107. <https://doi.org/10.1016/j.jseas.2016.02.010>.
- Li, M., Simoneit, B., Zhong, N., Fang, R., 2013. The distribution and origin of dimethylbenzothiophenes in sediment extracts from the Liaohu Basin, East China. *Org. Geochem.* 65, 63–73. <https://doi.org/10.1016/j.orggeochem.2013.10.007>.
- Li, M., Wang, T., Shi, S., Zhu, L., Fang, R., 2014. Oil maturity assessment using maturity indicators based on methylated dibenzothiophenes. *Petrol. Sci.* 11, 234–246. <https://doi.org/10.1007/s12182-014-0336-3>.
- Li, J., Tang, Y., Wu, T., Zhan, J., Wu, H., Wu, W., Bai, Y., 2020. Overpressure origin and its effects on petroleum accumulation in the conglomerate oil province in Mahu Sag, Junggar Basin, NW China. *Petrol. Explor. Dev.* 47 (4), 726–739. [https://doi.org/10.1016/S1876-3804\(20\)60088-X](https://doi.org/10.1016/S1876-3804(20)60088-X).
- Liang, X., Xu, Z., Zhang, Z., Wang, W., Zhang, J., Lu, H., Zhang, L., Zou, C., Wang, G., Mei, J., Rui, Y., 2020. Breakthrough of shallow shale gas exploration in Taiyang anticline area and its significance for resource development in Zhaotong, Yunnan Province, China. *Petrol. Explor. Dev.* 47 (1), 12–29. [https://doi.org/10.1016/S1876-3804\(20\)60002-7](https://doi.org/10.1016/S1876-3804(20)60002-7).
- Liu, G., Chen, Z., Wang, X., Gao, G., Xiang, B., Ren, J., Ma, W., 2016. Migration and accumulation of crude oils from Permian lacustrine source rocks to Triassic reservoirs in the Mahu depression of Junggar Basin, NW China: constraints from pyrolytic nitrogen compounds and fluid inclusion analysis. *Org. Geochem.* 101, 82–98. <https://doi.org/10.1016/j.orggeochem.2016.08.013>.
- Liu, S., Gao, G., Jin, J., Gang, W., Xiang, B., 2022. Source rock with high abundance of C₂₈ regular sterane in typical brackish-saline lacustrine sediments: biogenic source, depositional environment and hydrocarbon generation potential in Junggar Basin, China. *J. Petrol. Sci. Eng.* 208, 109670. <https://doi.org/10.1016/j.petrol.2021.109670>.
- Ma, D., He, D., Li, D., Tang, J., Liu, Z., 2015. Kinematics of syn-tectonic unconformities and implications for the tectonic evolution of the hala'alat mountains at the northwestern margin of the Junggar Basin, central asian orogenic belt. *Geosci. Front.* 6 (2), 247–264. <https://doi.org/10.1016/j.gsf.2014.07.004>.
- Mi, L., Zhang, X., Ding, L., Du, J., Zhang, S., 2018. Distribution characteristics and exploration strategy of middle-shallow lithologic reservoirs in offshore mature exploration areas: a case study on Huizhou sag in the Pearl River Mouth Basin, China. *Petrol. Explor.* 23 (6), 10–19. <https://doi.org/10.3969/j.issn.1672-7703.2018.06.002> (in Chinese).
- Moldowan, J.M., Seifert, W.K., Gallegos, E.J., 1985. Relationship between petroleum composition and depositional environment of petroleum source rocks. *AAPG Bull.* 69 (8), 1255–1268. <https://doi.org/10.1306/AD462BC8-16F7-11D7-8645000102C1865D>.
- Murphy, M.T., McCormick, A., Eglinton, G., 1967. Perhydro- β -carotene in the green river shale. *Science* 157 (3792), 1040–1042. <https://doi.org/10.1126/science.157.3792.1040>.
- Peng, G., Wen, H., Liu, C., Huang, F., Xu, Y., Quan, Z., Liu, H., 2013. Practice of shallow oil and gas exploration in Zhu I depression of the pearl river mouth basin: a case from Pangyu4 sag. *Mar. Geol. Front.* 29 (3), 22–28. <https://doi.org/10.16028/j.1009-2722.2013.03.003> (in Chinese).
- Peters, K.E., 1986. Guidelines for evaluating petroleum source rock using programmed pyrolysis. *AAPG Bull.* 70 (3), 318–329. <https://doi.org/10.1306/94885688-1704-11D7-8645000102C1865D>.
- Peters, K.E., Moldowan, J.M., 1991. Effects of source, thermal maturity, and biodegradation on the distribution and isomerization of homohopanes in petroleum. *Org. Geochem.* 17 (1), 47–61. [https://doi.org/10.1016/0146-6380\(91\)90039-M](https://doi.org/10.1016/0146-6380(91)90039-M).
- Peters, K.E., Cassa, M.R., 1994. Applied source rock geochemistry: chapter 5: Part II. Essential elements. In: Magoon, L.B., Dow, W.G. (Eds.), *The Petroleum System — from Source to Trap*. AAPG Bulletin, pp. 93–120. <https://doi.org/10.1306/m60585c5>.
- Peters, K.E., Walters, C.C., Moldowan, J.M., 2005. *The Biomarker Guide: Biomarkers and Isotopes in Petroleum Systems and Earth History*. Seconded, vol. 2. Cambridge University Press, Cambridge, pp. 483–607. <https://doi.org/10.1017/cbo9781107326040.004>.
- Philp, R.P., Chen, J.H., Fu, J.M., Sheng, G.Y., 1992. A geochemical investigation of crude oils and source rocks from Biyang Basin, China. *Org. Geochem.* 18 (6), 933–945. [https://doi.org/10.1016/0146-6380\(92\)90060-B](https://doi.org/10.1016/0146-6380(92)90060-B).
- Qian, T., Yu, X., Wei, Y., Zhang, Q., 2018. Characteristics of hydrocarbon accumulation in the Jurassic Badaowan Formation of Maxi slope and its exploration direction. *Petrol. Geol. Recov. Eff.* 25 (5), 32–38. <https://doi.org/10.13673/j.cnki.cn37-1359/te.2018.05.005> (in Chinese).
- Radke, M., Welte, D.H., Willsch, H., 1986. Maturity parameters based on aromatic hydrocarbons: influence of the organic matter type. *Org. Geochem.* 10 (1–3), 51–63. [https://doi.org/10.1016/0146-6380\(86\)90008-2](https://doi.org/10.1016/0146-6380(86)90008-2).
- Shanmugam, G., 1985. Significance of coniferous rain forests and related organic matter in generating commercial quantities of oil, Gippsland Basin, Australia. *AAPG Bull.* 69 (8), 1241–1254. <https://doi.org/10.1306/AD462BC3-16F7-11D7-8645000102C1865D>.
- Song, T., Huang, F., Wang, S., Yang, F., Lv, W., Ce, L., Peng, J., Fan, J., 2019. Characteristics and exploration potential of Jurassic oil and gas reservoirs in Mahu sag of the Junggar Basin, China. *Petrol. Explor.* 24 (3), 341–350. <https://doi.org/10.3969/j.issn.1672-7703.2019.03.007> (in Chinese).
- Tang, Y., Guo, W., Wang, X., Bao, H., Wu, H., 2019. A new breakthrough in exploration of large conglomerate oil province in Mahu Sag and its implications. *Xinjing Pet. Geol.* 39 (2), 127–137. <https://doi.org/10.7657/XJPG20190201> (in Chinese).
- Taylor, F.B., 1967. Outlook for shallow oil exploration and development, United States. *AAPG Bull.* 51 (1), 134–141. <https://doi.org/10.1306/5D25B79D-16C1-11D7-8645000102C1865D>.
- Ten Haven, H.L., Rohmer, M., Rullkötter, J., Bissert, P., 1989. Tetrahymanol, the most likely precursor of gammacerane, occurs ubiquitously in marine sediments. *Geochem. Cosmochim. Acta* 53 (11), 3073–3079. [https://doi.org/10.1016/0016-7037\(89\)90186-5](https://doi.org/10.1016/0016-7037(89)90186-5).
- Tissot, B.P., Welte, D.H., 1984. *Petroleum Formation and Occurrence*. Springer, Berlin.
- Volkman, J.K., 1988. Biological marker compounds as indicators of the depositional environments of petroleum source rocks. *Geological Society, London, Special Publications* 40 (1), 103–122. <https://doi.org/10.1144/GSL.SP.1988.040.01.10>.
- Volkman, J.K., Barrett, S.M., Dunstan, G.A., Jeffrey, S.W., 1994. Sterol biomarkers for microalgae from the green algal class Prasinophyceae. *Org. Geochem.* 21 (12), 1211–1218. [https://doi.org/10.1016/0146-6380\(94\)90164-3](https://doi.org/10.1016/0146-6380(94)90164-3).
- Wan, L., Liu, J., Mao, F., Lv, M., Bang, L., 2014. The petroleum geochemistry of the termit Basin, Eastern Niger. *Mar. Petrol. Geol.* 51, 167–183. <https://doi.org/10.1016/j.marpetgeo.2013.11.006>.
- Wang, D.Y., Li, M.J., Yang, L., Yang, Y., Li, E., Jin, J., Zou, X., Xu, B., 2022. The distribution of triaromatic steroids in Permian source rocks and implications for oil-source correlations in the Mahu Sag, Junggar Basin, NW China. *Nat. Gas Geosci.* 33 (11), 1862–1873. <https://doi.org/10.11764/j.issn.1672-1926.2022.06.010> (in Chinese).
- Wang, T., Cao, J., Carroll, A.R., Zhi, D., Tang, Y., Wang, X., Li, Y., 2021. Oldest preserved sodium carbonate evaporite: late paleozoic Fengcheng Formation, Junggar Basin, NW China. *GSA Bull.* 133 (7–8), 1465–1482. <https://doi.org/10.1130/B35727.1>.
- Wang, X., Wang, Y., Guan, D., Li, C., Liu, P., 2012. Shallow petroleum geology and exploration potential in the slope area, circum-Bozhong Sag, China Offshore Oil Gas 24 (3), 12–16. <https://doi.org/10.3969/j.issn.1673-1506.2012.03.003> (in Chinese).
- Wu, K., Qu, J., Wang, H., 2014. Strike-slip characteristics, forming mechanisms and controlling reservoirs of Dazhuluogou fault in Junggar Basin. *J. China Univ. Petrol. (Ed Nat Sci)*. 38 (5), 41–47. <https://doi.org/10.3969/j.issn.1673-5005.2014.05.006> (in Chinese).
- Wu, W., Li, Q., Pei, J., Ning, S., Tong, L., Liu, W., Feng, Z., 2020. Seismic sedimentology, facies analyses, and high-quality reservoir predictions in fan deltas: a case study of the Triassic Baikouquan Formation on the western slope of the Mahu Sag in China's Junggar Basin. *Mar. Petrol. Geol.* 120, 104546. <https://doi.org/10.1016/j.marpetgeo.2020.104546>.
- Xia, L., Cao, J., Bian, L., Hu, W., Wang, T., Zhi, D., Tang, Y., Li, E., 2022. Co-evolution of paleo-environment and bio-precursors in a Permian alkaline lake, Mahu mega-oil province, Junggar Basin: implications for oil sources. *Sci. China Earth Sci.* 65, 462–476. <https://doi.org/10.1007/s11430-021-9861-4>.
- Xiao, Z., Chen, S., Liu, C., Lu, Z., Zhu, J., Han, M., 2021. Lake basin evolution from early to middle permian and origin of triassic baikouquan oil in the western margin of Mahu sag, Junggar Basin, China: evidence from geochemistry. *J. Petrol. Sci. Eng.* 203, 108612. <https://doi.org/10.1016/j.petrol.2021.108612>.
- Yang, F., Wang, T., Li, M., 2015. The distribution of triaromatic steroids and oil group classification of Ordovician petroleum systems in the cratonic region of the Tarim Basin, NW China. *Petrol. Sci. Technol.* 33 (12), 1794–1800. <https://doi.org/10.1080/10916466.2015.1092984>.
- Yang, F., Yun, L., Wang, T.G., Ding, Y., Li, M., 2017. Geochemical characteristics of the Cambrian source rocks in the Tarim Basin and oil-source correlation with

- typical marine crude oil. *Oil Gas Geol.* 38 (5), 851–861. <https://doi.org/10.11764/j.issn.1672-1926.2016.05.0861> (in Chinese).
- Yu, K., Cao, Y., Qiu, L., Sun, P., 2018. The hydrocarbon generation potential and migration in an alkaline evaporite basin: the Early Permian Fengcheng Formation in the Junggar Basin, northwestern China. *Mar. Petrol. Geol.* 98, 12–32. <https://doi.org/10.1016/j.marpetgeo.2018.08.010>.
- Zhang, B., Li, M., Zhao, Q., Wang, T., Zhang, K., Xiao, Z., Huang, S., 2016. Determining the relative abundance of C₂₆–C₂₈ triaromatic steroids in crude oils and its application in petroleum geochemistry. *Petrol. Geo. Exper.* 38 (5), 692–697. <https://doi.org/10.11781/sydydz201605692> (in Chinese).
- Zhao, J., Chen, S., Deng, G., Shao, X., Zhang, H., Aminov, J., Chen, X., Ma, Z., 2019. Basement structure and properties of the western Junggar Basin, China. *J. Earth Sci.* 30, 223–235. <https://doi.org/10.1007/s12583-018-1207-4>.
- Zhang, Z., Gu, Y., Jin, J., Li, E., Yu, S., Pan, C., 2022. Assessing source and maturity of oils in the Mahu sag, Junggar Basin: molecular concentrations, compositions and carbon isotopes. *Mar. Petrol. Geol.* 141, 105724. <https://doi.org/10.1016/j.marpetgeo.2022.105724>.
- Zhi, D., Tang, Y., He, W., Guo, X., Zheng, M., Huang, L., 2021. Orderly coexistence and accumulation models of conventional and unconventional hydrocarbons in lower permian Fengcheng Formation, Mahu sag, Junggar Basin. *Petrol. Explor. Dev.* 48 (1), 43–59. [https://doi.org/10.1016/S1876-3804\(21\)60004-6](https://doi.org/10.1016/S1876-3804(21)60004-6).
- Zumberge, J.E., 1987. Terpenoid biomarker distributions in low maturity crude oil. *Org. Geochem.* 11 (6), 479–496. [https://doi.org/10.1016/0146-6380\(87\)90004-0](https://doi.org/10.1016/0146-6380(87)90004-0).